Bioorg. Med. Chem. 99 (2024) 117563

Contents lists available at ScienceDirect

Bioorganic & Medicinal Chemistry

journal homepage: www.elsevier.com/locate/bmc

Synthesis, structural study and antitumor activity of novel alditol-based imidazophenanthrolines (*aldo*-IPs)

Ana Gómez-Bra [a,b], Lourdes Gude [a,b,*], María-Selma Arias-Pérez [a,*]

[a] Universidad de Alcalá, Departamento de Química Orgánica y Química Inorgánica, Instituto de Investigación Química "Andrés M. del Río" (IQAR), 28805-Alcalá de Henares, Madrid, Spain
[b] Grupo DISCOBAC, Instituto de Investigación Sanitaria de Castilla-La Mancha (IDISCAM), Spain

ARTICLE INFO

Keywords:
Carbohydrate-based derivatives
Alditol-imidazophenanthrolines
Chiral polyhydroxy alkyl chains
Aerobic oxidative condensations
Antitumor agents

ABSTRACT

A series of 1*H*-imidazo [4,5-f][1,10] phenanthroline derivatives functionalized at 2-position with chiral, and conformationally flexible polyhydroxy alkyl chains derived from carbohydrates (alditol-based imidazophenanthrolines, *aldo*-IPs) is presented herein. These novel glycomimetics showed relevant and differential cytotoxic activity against several cultured tumor cell lines (PC3, HeLa and HT-29), dependent on the nature and stereochemistry of the polyhydroxy alkyl chain. The mannose-based *aldo*-IP demonstrated the higher cytotoxicity in the series, substantially better than cisplatin metallo-drug in all cell lines tested, and better than G-quadruplex ligand 360A in HeLa and HT29 cells. Cell cycle experiments and Annexin V-PI assays revealed that *aldo*-IPs induce apoptosis in HeLa cells. Initial study of DNA interactions by DNA FRET melting assays proved that the *aldo*-IPs produce only a slight thermal stabilization of DNA secondary structures, more pronounced in the case of quadruplex DNA. Viscosity titrations with CT dsDNA suggest that the compounds behave as DNA groove binders, whereas equilibrium dialysis assays showed that the compounds bind CT with K_a values in the range 10^4–10^5 M^{-1}. The *aldo*-IP derivatives were obtained with synthetically useful yields through a feasible one-pot multistep process, by aerobic oxidative cyclization of 1,10-phenanthroline-5,6-diamine with a selection of unprotected aldoses using $(NH_4)_2SO_4$ as promoter.

1. Introduction

Heterocycles coupled with carbohydrate moieties have become promising multitarget compounds with practical prospects. The characteristics and structural variety of both domains allow the control of the biocompability and functions of the resulting conjugated and/or hybrid compounds.[1–4] Small multifunctional compounds suitably functionalized have currently attracted much attention as versatile materials with novel chemical features and properties. Among the different strategies so far explored, those based on the combination of several active units are particularly effective due to the possibility of modulating the properties of these derivatives through structural variations in distinct frameworks, in an attempt to provide synergistic effects of the different domains.

In this field, molecular hybrids and conjugates bearing carbo- and heterocyclic-fused imidazoles have been extensively studied because of their synthetic utility and variety of applications.[5–10] Among them, imidazophenanthroline derivatives (IPs) and their metal complexes are attractive moieties for the development of functional materials and multifunctional compounds with high multimodal therapeutic performance acting as antiviral, anti-inflammatory, antibacterial or anticancer agents.[7–9] It has been reported that IP derivatives can inhibit the proliferation of tumor cells by diverse mechanisms, such as stabilization of G-quadruplex DNA, DNA photocleavage via formation of reactive oxygen species (ROS) or inhibition of DNA synthesis.[7,9,11,12]

Carbohydrates are well known by their structural diversity and characteristics, including availability, high water-solubility and optical activity. Due to their site-specific character, oligosaccharides and glycoconjugates present on the cellular surface are associated with specific biological recognition, targeting and signalling processes that play important roles in both normal and disease states.[4] Many carbohydrates are known to be good binders for nucleic acids, and it has been shown they are potential motifs for selective G-quadruplex recognition.[13–15] Several carbohydrate-functionalized derivatives have been proven to be

* Corresponding authors at: Universidad de Alcalá, Departamento de Química Orgánica y Química Inorgánica, Instituto de Investigación Química "Andrés M. del Río" (IQAR), 28805-Alcalá de Henares, Madrid, Spain.
E-mail addresses: lourdes.gude@uah.es (L. Gude), selma.arias@uah.es (M.-S. Arias-Pérez).

https://doi.org/10.1016/j.bmc.2023.117563
Received 5 July 2023; Received in revised form 17 November 2023; Accepted 18 December 2023
Available online 21 December 2023

excellent G-quadruplex ligands and/or exhibit relevant antitumor activity, which makes them interesting compounds from the perspective of anticancer therapies.[13–15] Additionally, the conjugation of multivalent derivatives with carbohydrates could enhance the targeting efficacy of an anticancer agent by promoting the selective uptake in tumor cells, taking advantage of the "Warburg effect" and energy requirements displayed by cancerous cells.[16]

Moreover, carbohydrates have been used as natural reagents for the synthesis of new materials, especially aromatic *N*-heterocycles, such as pyrimidines, pyrazines, imidazoles, benzimidazoles, naphtimidazoles or quinoxalines.[17,18] Many carbohydrate-based derivatives have been applied in medicinal chemistry as antibiotic, antiviral or antitumor therapeutics, glycosylation inhibitors, diagnostic agents, pathologic probes and key structural units in vaccines.[3,19] On the other hand, modification of the base or sugar components of nucleosides is a valuable strategy to find helpful analogues.[19c,20,21] This is the case of the antiviral remdesivir (GS-5734), an inhibitor of the viral RNA-dependent polymerase used for the treatment of COVID-19,[20] and [^{18}F]FAZA ([^{18}F]fluoro-azomycin-α-arabinoside), a 2-nitroimidazole (azomycin) sugar derivative -mimicking nucleosides-, acting as a PET radiotracer clinically applied in diagnosing a wide range of solid tumors.[21]

Bearing in mind these reports, we are involved in the development of carbohydrate-based heteroaromatic hybrids that could bind/or interact with DNA structures as potential antitumor agents.[14] Herein, the synthesis and characterization of a novel series of chiral 1*H*-imidazo[4,5-f][1,10]phenanthroline derivatives functionalized at 2-position with a linear polyhydroxy alkyl chain of five or four carbons, derived from carbohydrates -alditol moiety- are presented (Scheme 1). These *aldo*-imidazophenanthrolines (*aldo*-IPs) were prepared through a one-pot multistep synthesis by aerobic oxidative cyclization of 1,10-phenanthroline-5,6-diamine with a selection of unprotected aldoses (D-glucose, D-galactose, D-mannose, 2-deoxy-D-glucose, L-rhamnose, L-xylose, D-arabinose, D-ribose). Initial studies of DNA interactions and preliminary evaluation of cytotoxic activity against several cultured tumor cell lines of these alditol-based imidazophenanthrolines are included. Compared to the previously described family of *N*-4-(1*H*-imidazo[4,5-f][1,10]phenanthrolin-2-yl)phenyl-β-glycopyranosylamines (*carb*-APIPs),[14a] the new ligands retain the extended π-conjugated IP fragment, which can bind to duplex DNA and G-4 DNA structures through π-stacking. However, the rigid cyclic substituent at 2-position has been replaced by a flexible linear polyhydroxy alkyl chain, in which the structural integrity of the parent carbohydrate is lost. These changes may provide uselful information about the influence of carbohydrate structure and flexibility on biological activity. Most reported DNA ligands possess a rigid structure and less attention has been paid to conformationally flexible ones. However, it has been suggested that a high rotational flexibility of the ligands should increase the number of the possible binding modes with DNA structures, owing to their ability to adopt diferent conformations depending on the target, improving the binding affinity and/or selectivity.[1c,1d,22] Among the variety of sugar analogues, open chain sugar alcohols –alditols- present interesting properties.[3b,17,23] They retain water-solubility and optical activity, but have high stability to heat and acids, are not prone to Maillard reaction and are more resistant to be digested and degraded by the enzyme system in the body.[3b] Thus, the natural product rivoflavin (vitamin B_2), an essential coenzyme for redox reactions in many different metabolic pathways, displays a polyhydroxy carbon chain and a pyrimidine-fused heterocycle in its structure.[23]

2. Results and discussion

2.1. Synthesis and structural study

Owing to the interesting properties of suitable functionalized imidazoles and carbo- or heterocyclic-fused derivatives, the development of efficient synthetic routes for their preparation has received much attention.[5c,d,6,18,24–26] One conventional method involves the oxidative condensation of an aliphatic or aromatic aldehyde with 1,2-diamines in the presence or absence of a catalyst and/or an oxidizing agent. Strong acids or harsh reaction conditions are often used and extensive efforts have been devoted to finding sustainable and straightforward methodologies. In this regard, iodine promoted and metal-free aerobic oxidative protocols have been reported for benzimidazole synthesis.[18,24,25] Lin *et al.* have also found that *aldo*-benzimidazoles and *aldo*-naphtimidazoles can be efficiently prepared by I_2-catalyzed oxidative condensation of aldoses with the respective aromatic 1,2-diamine in acetic acid solution.[18]

It has been proposed that the construction of the imidazole cycle, from aldehydes or aldoses and 1,2-diamines was initiated, as the *N*-glycosylation reactions, by formation of a Schiff base through condensation of the carbonyl moiety with one of the amino groups in the 1,2-diamine.[5c,d,6,18,24–26] The cyclization of the imine intermediate with participation of the other amino group would form an imidazoline, which could be oxidized in air or by an oxidant to give the imidazole derivative. Working on these bases, we decided to explore the aerobic

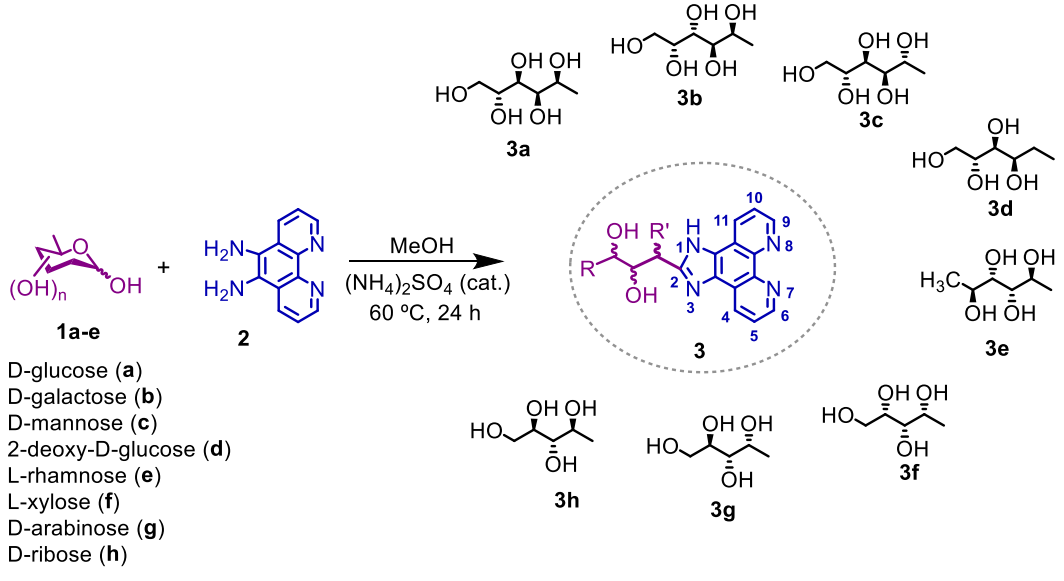

Scheme 1. Synthesis and structure of the chiral 2-polyhydroxyalkyl-1*H*-imidazo[4,5-f][1,10]phenanthrolines (*aldo*-imidazophenanthrolines, *aldo*-IPs) **3a–h.**

oxidative condensation of unprotected monosaccharides with 1,10-phenanthroline-5,6-diamine using a large excess of sugar and a catalytic amount of $(NH_4)_2SO_4$ as promoter in methanol (Scheme 1). These conditions were previously applied to the synthesis of *N*-heteroarylglycosylamines and *N*-glycopyranosyhydrazones with useful yields and excellent stereoselectivities.[14a,b,d]

In order to optimize the process, the reaction of 1,10-phenanthroline-5,6-diamine and D-glucose was carried at different conditions (Table 1). At room temperature, no reaction was observed, even after a long time (48 h, entry 1) and the starting materials were recovered intact. By heating at 60 °C, only traces of the imidazophenanthroline derivative **3a** (7–8 %) were formed at short reaction times and the *N*-(6-amino-1,10-phenanthrolyn-5-yl)-β-D-glucopyranosylamine (**4a**) was the major product (45 % and 85 % for 4 and 8 h, respectively). An increase of the reaction time led to higher yields of the *aldo*-IP **3a** and the conversion was practically quantitative at 60 °C for 24 h. Similar yields were found with 3 or 5 equiv. of sugar (entries 4 and 5). However, the yield of **3a** greatly decreased to 42 % in the absence of $(NH_4)_2SO_4$ and the monoglycosylamine **4a** was not detected. Using $(NH_4)_2SO_4$ as promoter in methanol at 60 °C for 24 h, the reactions of the monosaccharides tested with 1,10-phenanthroline-5,6-diamine afforded the corresponding oxidative condensation products (*aldo*-IPs **3a–h**) in moderate to high yields (48–92 %, Table 1). In all cases, the diamine **2** was exhausted and the lowest yields were due to loss of product during isolation and purification. Bis-glycosylamines, 1,2-disubstituted imidazophenanthrolines and/or other side-products were not detectable in yields higher than 3 %.

Based on these findings and previous mechanistic studies on related imidazole synthesis by oxidative cyclization,[18,24] this one-pot multistep process could take place through the reaction sequence drawn in Scheme 2. The experimental results strongly suggest that $(NH_4)_2SO_4$ plays a key role, by promoting the formation of a highly reactive imine intermediate (**B**), not detectable under the employed conditions. The Schiff base **B** could experience two alternative cyclizations: 1) by direct reaction of the other amino group with the imine moiety to give the imidazoline intermediate (**D**, Scheme 2, pathway a); 2) by nucleophilic addition of the OH group at 5-position in the polyhydroxy alkyl chain to afford an amino *N*-glycopyranosylamine (**4**) (Scheme 2, pathway b). Das *et al*[27] have described the preparation of a bis-glycosylamine in 61 % yield by heating at reflux 4,6-O-benzylidene-D-glucopyranose with *o*-phenylenediamine in ethanol solution for a short reaction time (15 min.) but they do not report the formation of the benzimidazole derivative. The involvement of the *N*-glycosylamine was not mentioned in the synthesis of *aldo*-benzimidazoles and *aldo*-naphtimidazoles by I_2-catalyzed oxidative condensation of aldoses in acetic acid solution.[18] The authors suggest that the *aldo*-imidazole products might originate through the Schiff base **B** by the direct addition of the amino group followed by oxidation of the imidazoline intermediate (**D**) or previous formation of an *N*-iodoimidazoline intermediate by *N*-iodination of the carbon–nitrogen double bond and subsequent elimination of HI. However, Lee *et al.*[24] have found that the synthesis of benzimidazoles from *o*-phenylenediamine and aldehydes *via* aerobic oxidation requires the presence of a nucleophile as I^-, water or an alcohol. They proposed that the nucleophilic catalyst acts promoting the cyclization of the imine through the conversion of 5-*endo-trig* direct cyclization, disfavoured by the Baldwin's rules,[28] to favoured 5-*exo-tet* cyclization *via* a tetrahedral intermediate generated by the addition of the nucleophile to the imine group. According to this study, the imine **B** should undergo 6-*exo-trig* cyclization, favoured by Baldwin's rules, rather than disfavoured 5-*endo-trig* cyclization to readily generate the *N*-glycosylamine **4**. This hypothesis was corroborated by the isolation of **4a** at short reaction times. Moreover, the *aldo*-IP **3a** was also obtained when derivative **4a** was directly subjected to the reaction conditions.

The formation of the imidazoline intermediate **D** might be the rate-determining step and could occur by different routes. The formation of the imine **B** and *N*-glycosylamine **4** are reversible processes and, according to previous studies,[24] intermediates **A** and **B** could lead to the imidazoline **D**. As the reactions were carried out in methanol solution, during the equilibrium the alcohol could act as a nucleophilic catalyst to generate the methoxy tetrahedral intermediate **C** that could provide the imidazoline **D** by a favoured 5-*exo-tet* cyclization (Scheme 2, pathway c). Similarly, the tetrahedral intermediate **A** would be susceptible to form **D** too. Moreover, the amino *N*-glycosylamine **4** could also undergo a favoured 5-*exo-tet* cyclization by nucleophilic attack of the amino group on the tetrahedral anomeric carbon affording **D** (Scheme 2, pathway d). As it was possible to stop the reaction sequence and isolate the amino *N*-glycosylamine **4**, the last alternative may be the most favourable pathway in our conditions. Finally, the aerobic oxidation of the unisolated imidazoline intermediate would furnish the *aldo*-IPs **3**. In this case, bis-glycosylamines **5** were not detected, and the high thermodynamic stability of the extended π-conjugated imidazophenanthroline system seems to be the driving force of this multistep reaction.

Table 1
Aerobic oxidative condensation of unprotected monosaccharides with 1,10-phenanthroline-5,6-diamine.[a]

Entry	Carbohydrate	Temperature (°C)/Reaction time (h)	*Aldo*-Imidazophenanthrolines (*Aldo*-IPs), yield (%)[b]
1	D-glucose	25/48	–[c]
2		60/4	**3a**, 7[d]
3		60/8	8[d]
4		60/24	89
5		60/24	90
6		60/48	42[e]
7	D-galactose	60/24	**3b**, 80
8	D-mannose	60/24	**3c**, 92
9	2-deoxy-D-glucose	60/24	**3d**, 90
10	L-rhamnose	60/24	**3e**, 67
11	L-xylose	60/24	**3f**, 48
12	D-arabinose	60/24	**3g**, 66
13	D-ribose	60/24	**3h**, 79

[a] Reaction conditions: catalytic $(NH_4)_2SO_4$ in methanol, molar ratio monosaccharide: diamine 3:1 except for entries 2–4, 5:1; [diamine] = 0.033 M.
[b] Yields of isolated products except for entries 2 and 3, in which cases the values correspond to the conversion of starting diamine and were determined by ^{1}H-NMR (±2 %) of the crude reaction mixture.
[c] No reaction was observed and the starting diamine was recovered.
[d] In these cases it was observed the formation of the *N*-(6-amino-1,10-phenanthrolyn-5-yl)-β-D-glucopyranosylamine (**4a**) as the major product (45 % and 85 % for 4 and 8 h, respectively).
[e] The reaction was carried in the absence of $(NH_4)_2SO_4$.

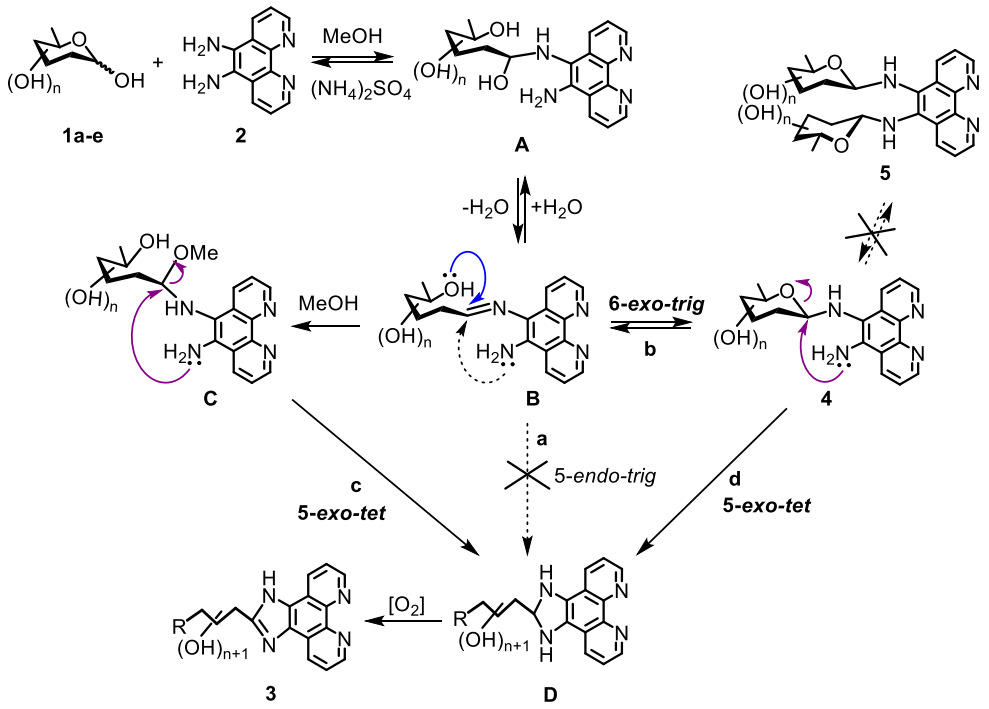

Scheme 2. Plausible reaction sequence for the one-pot multistep synthesis of the *aldo*-imidazophenanthrolines **3** by aerobic oxidative cyclization.

The *aldo*-IP derivatives **3a–h** were studied in depth by ^{1}H and ^{13}C NMR in $(CD_3)_2SO$ and $(CD_3)_2SO$-D_2O using homonuclear and heteronuclear 2D-NMR techniques for the identification and unambiguous assignment of the proton and carbon resonances (Figs. S3–S33). At 500 MHz, the ^{1}H NMR spectra in $(CD_3)_2SO$ showed low resolution and greater complexity in the region around 3.0–6.0 ppm, where most signals of the polyhydroxy alkyl chains appear. In general, better resolution was observed in $(CD_3)_2SO$-D_2O, and the aliphatic proton signals were simplified since, in these conditions, the vicinal coupling constants with OH protons were removed. The interpretation of the ^{1}H–^{1}H COSY and TOCSY spectra was based on the unambiguous assignment of the signals corresponding to H-1′ that, except in the case of **3d**, appeared around 5.0 ppm as a doublet of doublets in $(CD_3)_2SO$ and a doublet in $(CD_3)_2SO$-D_2O, CH_2 protons, or CH_3 group in **3e,** owing to their shape and chemical shifts. Imidazolyl NH proton was observed as a singlet about 13.4 ppm. Aromatic protons in *aldo*-IPs resonate around 9.0–7.8 ppm, showing a slightly greater deshielding (Δδ 0.2–0.5 ppm) than those in diamine **2.** The unequivocal assignment of all carbon resonances was based on the chemical shifts found for related systems and the analysis of the direct and long-range ^{1}H–^{13}C correlated spectra (gC2HSQCSE, gHMBC), once the signals of the respective protons were established. Compared to precursor diamine, aromatic carbons of the phenanthroline moiety also appear deshielded in *aldo*-IPs, being the effect higher for C-6 (9) and C-7a(7b) (Δδ ~ 2 ppm). In *aldo*-IPs chemical shifts and shape of the phenanthroline proton signals are dependent on the solvent and concentration; H-4/H-11 (see Scheme 1 for numbering) resonate as one or two broadened signals with small Δδ, while H-5/H-10 and H-6/H-9 become chemically equivalent. Concerning the carbon atoms, the imidazo[4,5-f][1,10]phenanthroline group give broadened and weak signals -except C-2 and C-6(9) around 156.0 at 147.0 ppm, respectively- Moreover, excluding C-2 and C-7a(7b), quaternary carbons beyond detection in practically all cases and could not be observed even in the gHMBC ^{1}H–^{13}C correlation spectra (Figs. S5 and S9). This behavior suggests an intermediate exchange rate for the imidazole prototropic taumerism.[9i,14a,29] Data are collected in Table 2 and in the experimental section.

In the polyhydroxy alkyl chain of the *aldo*-IPs, the stereogenic centers retain the configuration of the sugar precursors because only the anomeric carbon was involved in the formation of the imidazole ring. Conformational properties of different carbohydrate-derived polyols

Table 2
Selected NMR parameters of the 2-polyhydroxyalkyl-1*H*-imidazo[4,5-f][1,10] phenanthrolines **3a–h** in $(CD_3)_2SO$-D_2O.

	3a	3b	3c	3d	3e	3f	3g	3h
δ (ppm)								
H-1′	5.07	5.29	4.92	3.12;3.17	4.90	5.08	5.28	5.11
H-2′	4.15	3.98	4.20	4.35	4.21	3.95	3.88	3.93
H-3′	3.36	3.69	3.76	3.30	3.51	3.53	3.67	3.65
H-4′	3.54	3.79	3.55	3.55	3.65	3.45;3.53	3.50;3.67	3.46;3.62
H-5′	3.34;3.56	3.44;3.49	3.46;3.68	3.43;3.63	1.17			
C-1′	70.2	67.7	68.1	33.5	68.0	69.2	67.8	69.5
C-2	155.2	156.4	156.4	155.4	156.4	155.7	155.9	155.2
J (Hz)								
$^{3}J_{H1'\text{-}H2'}$	6.4	1.7	8.9	8.8;5.1	8.8	5.3	2.0	5.2
$^{3}J_{H2'\text{-}H3'}$	1.9	9.4	1.0	1.4	1.2	3.1	8.2	6.7
$^{3}J_{H3'\text{-}H4'}$	8.1	1.5	8.7	8.5	8.3	5.4;5.3[a]	6.7[a];-	6.2;3.4
$^{3}J_{H4'\text{-}H5'}$	5.7;3.4	6.6;6.6	6.1;3.3	6.0;3.4	6.2			

[a] Values in $(CD_3)_2SO$.

have been studied in detail and many factors are considered to influence their behavior, including steric interactions, the gauche effect, solvent effects and, predominantly, the cooperative effect of intra- and intermolecular hydrogen bonding.[30,31] It is usually assumed that rotation about the C-C bonds in the polyhydroxy alkyl chain of a sugar alcohol is sufficiently unrestricted that a mixture of staggered conformers could exist in solution. NMR spectroscopic studies of acyclic sugar derivatives in solution have provided data consistent with the hypothesis that the acyclic carbon chains have the extended, planar, zigzag arrangement, unless this spatial disposition would give rise to steric 1,3-parallel interactions.[30] If such interactions are present, the carbon chain would adopt a bent conformation so that these interactions were avoided. In a planar, linear zigzag conformation for the 1,2-dihydroxy dimethine systems (internal C-C bonds) of a polyol the vicinal $^3J_{HH}$ coupling constants should be either small (<3 Hz) or large (7–10 Hz), as the neighboring protons are positioned either in a *gauche* or *anti* orientation.[30a–f] Intermediate $^3J_{HH}$ coupling constants (3–7 Hz) instead have been attributed to the contribution of *gauche/anti* equilibrating rotamers or are associated with a bent non-planar conformation by rotation of the linear carbon chain in solution.[30a–f] Thus, it was shown that galactose-, mannose- and arabinose-based polyols have essentially planar carbon chains - both in the solid state and in solution- and the vicinal coupling constants follow a regular pattern, being either small (1–2 Hz) when the neighboring protons are in *gauche* orientation, or large (8.1–9.5 Hz) when the neighboring protons are in *anti* disposition.[30a,b,d–g,31b] However, the intermediate values for $^3J_{H2\text{-}H3}$ in glucitol were attributed to a twisted conformation at C2-C3 fragment.[30d–g] In the case of xylitol and ribitol it was proposed that they equilibrate between a twist conformation at C2-C3 and one at C3-C4.[30c,f,g,31b] In the case of ribitol a bent carbon chain was observed in the solid state and in the gas phase five conformations have been identified, two with extended carbon chains and three with bent chains.[30c,31b]

For all *aldo*-IPs prepared, the $^3J_{HH}$ coupling constant patterns of the polyol backbone (Table 2) are in perfect agreement with those reported earlier for the original polyols derived from the precursor sugar. The observed values did not exhibit any significant solvent-dependence ($(CD_3)_2SO$-D_2O and $(CD_3)_2SO$ solutions) and indicate that the conformational behavior of the polyhydroxylated carbon chain of the related alditols is practically retained in derivatives **3a–h**. In compounds **3b,c** the values of coupling constants $^3J_{H1'\text{–}H2'}$, $^3J_{H2'\text{–}H3'}$ and $^3J_{H3'\text{-}H4'}$ are similar to those of $^3J_{H2\text{-}H3}$, $^3J_{H3\text{-}H4}$ and $^3J_{H4\text{-}H5}$ coupling constants observed in galactitol and mannitol[30a,b,d–g,31b]; in **3g** $^3J_{H1'\text{–}H2'}$ and $^3J_{H2'\text{–}H3'}$ are in concordance with the $^3J_{H2\text{-}H3}$ and $^3J_{H3\text{-}H4}$ of arabinitol.[30d–g,31b] These observations agree with a planar and linear conformation of the C1′-C2′-C3′-C4′ and C1′-C2′-C3′ fragments in **3b,c** and **3g**, respectively. The same arrangement can be proposed for the C1′-C2′-C3′-C4′ segment in **3e**.[31b] Like glucitol,[30d–g,31b] *aldo*-IPs **3a,d** exhibited a linear conformation for the C2′-C3′-C4′ chain, but the C1′-C2′ system of **3a** would mainly adopt a bent form, to avoid the 1,3-parallel interaction between OH-1′ and OH-3′. However, **3f,h**, as xylitol and ribitol,[30c,f,g,31b] can be described by a pair of equilibrating rotamers twisted at C1′-C2′ or C2′-C3′ bonds, so removing the OH-1′/OH-3′ present in the planar chain form. The intermediate $^3J_{HH}$ values (3.4–6.7 Hz) observed for the terminal C-C segment (C4′-C5′ or C3′-C4′) suggest conformational averaging by an equilibrium between its three staggered conformations -two *gauche* and one *anti* rotamers.[30c-g]

2.2. Cytotoxic activity, cell cycle and apoptosis assays

It has been reported that IP derivatives can inhibit the proliferation of tumor cells by diverse mechanisms.[7,9] As an illustration, it has been found that the unsubstituted 1*H*-imidazo[4,5-f][1,10]phenanthroline can interfere with the PI3K/AKT/mTOR signaling pathway and might be a potential therapeutic candidate for the treatment of colorectal cancer,[7c] while fluorinated imidazole[4,5f][1,10]phenanthroline derivatives, particularly 2-(2,3-difluorophenyl)-1*H*-imidazo[4,5-f][1,10]phenanthroline, may inhibit cell proliferation of liver cancer cells *in vitro* and *in vivo*, by inducing apoptosis via DNA damage.[7d] The family of 2-aryl-imidazo[4,5-f][1,10]phenanthroline conjugates (*carb*-APIPs) has shown a significant ability to bind telomeric G-quadruplex DNA, with the carbohydrate motif playing a crucial role in the quadruplex versus duplex DNA selectivity observed.[14a] In addition, these *carb*-APIPs, especially in the case of the rhamnose derivative, showed significant cytotoxic properties in PC3 and HeLa and, to a lesser extent, in MCF7 and normal human fibroblasts (HFF1) cultured cells. Moreover, uracil-alditol derivatives having a porphyrin unit have shown photodynamic efficiency against prostate cancer cell line,[17b] and alditol-indenoisoquinolines have displayed potent topoisomerase I poisoning and antiproliferative activities, dependent upon stereochemistry.[17e] However, little systematic work about the potential antitumor activity of alditol-based heterocyclic derivatives has been described in the literature.

In the present work, the cytotoxic activity in cultured cells of the novel *aldo*-IPs has been preliminary tested in PC3 (prostate), HeLa (cervix) and HT29 (colorectal adenocarcinoma) cancer cells and in normal human fibroblast (HFF1) cells, by the MTT assay after a 72 h treatment (Table 3, Figs. S34–S39). As reference compounds to establish comparisons with previous studies, G-quadruplex ligand 360A and cisplatin were considered.

The *aldo*-IPs **3a–h** showed relevant cytotoxicity in PC3, HeLa and HT29 tumor cell lines, with IC_{50} values in the micromolar concentration range. Although their relative activity is dependent on the cell line tested, overall, the mannose-based *aldo*-IP (**3c**) demonstrated the higher cytotoxicity in the series, followed by the galactose and rhamnose *aldo*-IPs (**3b** and **3e**, respectively) and the glucose *aldo*-IP (**3a**). The cytotoxicity of **3c** is substantially higher than cisplatin metallo-drug in all cell lines tested, and also higher than 360A in HeLa and HT29 cells. In general, the cytotoxic potency of the *aldo*-IP family in cultured cells

Table 3
Cytotoxic activity of compounds **3a–h** and selected controls in PC3, HeLa, and HT29 tumor cells and in normal fibroblast (HFF1) cells after 72 h incubation.

	PC3	Hela	HT29	HFF1	SI[a]
Compound (precursor)	IC_{50} (μM)	IC_{50} (μM)	IC_{50} (μM)	IC_{50} (μM)	
3a (glucose)	14.3 ± 3.5	9.7 ± 1.9	64.2 ± 1.6	47.1 ± 4.9	3.3
3b (galactose)	17.8 ± 3.9	15.4 ± 3.2	13.1 ± 1.3	73.4 ± 14.6	4.1
3c (mannose)	6.3 ± 0.6	6.4 ± 0.3	14.2 ± 1.4	15.9 ± 2.4	2.5
3d (2-deoxy-D-glucose)	17.6 ± 5.8	35.6 ± 5.2	63.4 ± 2.8	>300	>17
3e (rhamnose)	10.3 ± 3.0	14.8 ± 1.7	25.3 ± 1.6	14.4 ± 3.0	1.3
3f (xylose)	41.0 ± 5.6	40.6 ± 3.5	35.4 ± 2.1	>300	>7.3
3g (arabinose)	20.6 ± 2.7	11.7 ± 1.4	44.9 ± 5.4	33.4 ± 1.9	1.6
3h (ribose)	22.2 ± 7.7	71.1 ± 4.8	66.9 ± 15.3	>300	>13.5
360A[b]	2.5 ± 0.8	8.5 ± 1.4	>100	30.6 ± 2.3	12.2
Cisplatin[b]	12.8 ± 0.9	18.0 ± 1.9	86.6 ± 7.0	36.4 ± 4.4	2.8

[a] SI (Safety or selectivity index) determined as IC_{50} (HFF1)/IC_{50} (PC3).
[b] IC_{50} values for reference compounds 360A and cisplatin for PC3, Hela and HFF1 were determined under equivalent experimental conditions.[14a]

compares well with that observed for cisplatin and, although they are overall less cytotoxic than compound 360A in HeLa and PC3, all derivatives have lower IC_{50} values in the HT29 cell line than the reference compounds. At the same time, they also have proven cytotoxic in normal fibroblasts cells (HFF1), in some cases to a lower extent than in PC3 and HeLa cells, which confers some of the compounds with interesting selectivity. This is the case of the 2-deoxyglucose, xylose and ribose derivatives, **3d**, **3f** and **3h**, which displayed selectivity indexes, determined as IC_{50} (HFF1)/IC_{50} (PC3), of at least 17-, 7- and 13-fold, respectively. The lower cytotoxicity of *aldo*-IPs **3a–h**, compared to the *carb*-APIPs previously reported,[14a] might be associated with a diminished conjugation in the heteroaromatic moiety and the loss of the structural integrity of the precursor sugars by the replacement of the rigid and cyclic pyranoside by a flexible linear polyhydroxy alkyl chain.

Aldo-IPs **3a**, **3c**, **3d** and **3e** (derived from glucose, mannose, 2-deoxyglucose and rhamnose, respectively) were selected and further studied in cell cycle arrest assays using flow cytometry. Alterations in the cell cycle distribution (SubG0, G0/G1, S or G2/M populations) in HeLa and PC3 cells, after treatment with the compounds at ½ IC_{50} concentrations, for 72 h, were analyzed. It was found that, in HeLa cells, the *aldo*-IPs significantly increased the SubG0 population, suggestive of apoptosis, while they decreased the percentage of cells in the G0/G1 phase (Fig. S40). At the same time, minimal alterations in cell cycle distribution were observed for the *aldo*-IPs or positive control 360A tested in PC3 cells, under the analogous experimental conditions.

Additional cell cycle experiments, combined with the Annexin V-PI apoptosis assay, were run in HeLa cells (Fig. 1). The cells were subjected to treatment with the selected *aldo*-IPs at 10 μM concentration for 48 h, and cell cycle and early stage apoptosis were analyzed in parallel, using flow cytometry. As it can be observed in Figs. 1 and S41, all derivatives demonstrated to have pro-apoptotic effects in HeLa cells at low concentration. Cell cycle analysis confirmed a consistent increase in the SubG0 population, whereas the Annexin V-PI assay allowed to discern between the cell populations in early stage apoptosis and those in late apoptosis, compared to untreated cells used as controls. From the tested *aldo*-IPs, it was found that the compounds are able to induce apoptosis after 48 h, producing a higher increase in the number of early apoptotic cells. Interestingly, compound **3d**, the 2-deoxyglucose-derived alditol, showed the highest pro-apoptotic activity, comparable to that observed for antitumor compound 360A regarding total percentage of induced apoptosis, but significantly higher in terms of early stage apoptosis induction.

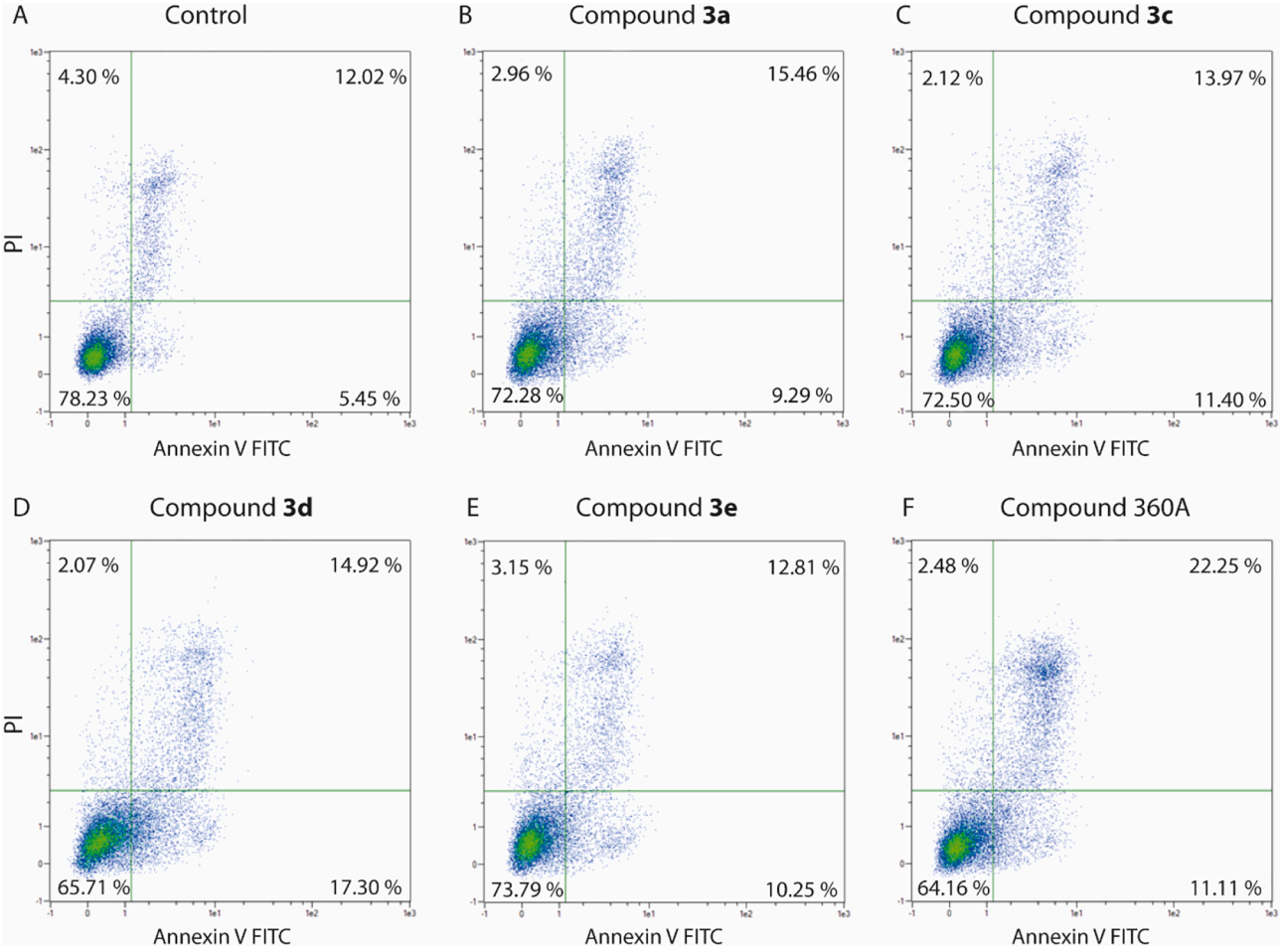

Fig. 1. Identification of apoptosis by the flow cytometry assay with Annexin V/PI double staining. HeLa cells were treated with *aldo*-IPs **3a**, **3c**, **3d**, **3e** or reference compound 360A, at 10 μM for 48 h. The lower left quadrants of the panels show the intact viable cells, the lower right quadrants represent apoptotic cells at early stage, the upper right quadrants show late stage apoptosis and the upper left quadrants represent necrotic cells. (A) Untreated cells; (B) Cells treated with **3a**; (C) Cells treated with **3c**; (D) Cells treated with **3d**; (E) Cells treated with **3e** and (F) Cells treated with 360A.

Table 4
Thermal stabilization of quadruplex DNA and dsDNA structures at 8 μM concentration of *aldo*-IPs.[a]

	G-DNA (F21T, K^+)	dsDNA (F10T)
Compound (precursor)	ΔT_m (°C)	ΔT_m (°C)
3a (glucose)	1.5 ± 0.5	0.0 ± 0.0
3b (galactose)	3.8 ± 0.3	1.5 ± 0.5
3c (mannose)	2.5 ± 0.5	1.0 ± 0.0
3d (2-deoxy-D-glucose)	1.5 ± 0.5	2.0 ± 0.0
3e (rhamnose)	3.5 ± 0.5	0.0 ± 0.0
3f (xylose)	3.8 ± 0.3	1.3 ± 0.3
3g (arabinose)	3.8 ± 0.3	1.0 ± 0.0
3h (ribose)	1.8 ± 0.3	0.5 ± 0.1

[a] ΔT_m values are the average of replicate measurements (±mean deviation).

2.3. DNA interactions

DNA interactions of *aldo*-IPs were preliminarily studied by FRET melting assays, by viscosity titrations and by equilibrium dialysis. The first type of experiment was carried out to detect possible thermal stabilization effects of the ligands on DNA secondary structures. For this purpose, short fluorescence-labelled oligonucleotide sequences, F10T and telomeric F21T, forming double-stranded or quadruplex structures, respectively, were selected. In addition, the non-covalent DNA binding mode was evaluated with Calf Thymus (CT) dsDNA, by testing the effect the *aldo*-IPs produce on the viscosity of DNA solutions. Targeting secondary structures and, in particular, DNA quadruplexes has currently many important applications. For example, it has recently proven to be an efficient strategy to develop compounds endowed with significant anticancer activity[12] and to explore directed bio-orthogonal synthetic methodologies promoted by DNA Templates.[32] Finally, equilibrium dialysis was used to determine apparent binding constants of selected *aldo*-IPs with CT DNA.

2.3.1. DNA FRET melting assays

Initial evaluation of *aldo*-IP-DNA interactions was carried out by FRET-based DNA melting assays[33] using a duplex forming oligonucleotide sequence designated as F10T and a representative example of a quadruplex sequence (F21T, human telomeric). Both oligonucleotide sequences tested are labeled with the fluorophore FAM at their 5′ end and the fluorophore TAMRA at the 3′ end. The experiments were carried out using folded (or annealed) DNA in the absence and in the presence of increasing concentrations of *aldo*-IPs, by slow heating from 25 °C to 95 °C, to determine T_m values (more precisely $T_{1/2}$ values).

In Table 4, the results obtained under the tested experimental conditions are shown. Overall, the *aldo*-IPs can modestly stabilize DNA secondary structures, at high [ligand]/[DNA] ratios, and the ΔT_m values determined for telomeric G4-DNA are slightly higher than for dsDNA. Compounds **3b**, **3e**, **3f** and **3g** (galactose, rhamnose, xylose and arabinose, Table 4 and Fig. S42) showed a slightly more pronounced stabilizing effect in the telomeric quadruplex structure, with ΔT_m values ~4 °C (8 μM). A more sublet effect on DNA denaturing was observed for the mannose derivative **3c**, whereas the rest of *aldo*-IPs, **3a**, **3d** and **3h** displayed weaker stabilization effects.

When *aldo*-IPs **3a–h** were tested for stabilization of double-stranded DNA, with the 10 bp sequence F10T (Table 4, Fig. S42), it was found that most of the compounds do not appreciably affect DNA melting curves, with low ΔT_m values ~0–1 °C, for most derivatives, and ΔT_m values ~2 °C in the cases of **3b** and **3d**. Taken together, our results suggest that the *aldo*-IPs produce minimal thermal stabilization on the tested DNA secondary structures.

All in all, the novel *aldo*-IPs ligands are not as good G4 stabilizers as the previously reported *carb*-APIPs,[14a] endowed with an extended aromatic surface more adequate for π-π stacking interactions, but they are better G4 stabilizers than their *N*-(1,10-phenanthrolin-5-yl)-β-glycopyranosylamine counterparts,[14c] which lack the imidazole ring, reinforcing the established principle that increased aromatic surfaces enhance π-interactions with quadruplex structures. The lack of thermal stabilization effects on dsDNA is suggestive of an interaction that involves groove binding, as opposite of what it is commonly expected to occur if an intercalation mechanism, with the ligands inserting between DNA base pairs, was involved.

2.3.2. Viscosity titrations

Viscosity titrations using Calf Thymus (CT) DNA solutions in the presence of *aldo*-IPs were carried out to determine the interaction mode with double-stranded DNA. This technique is commonly used to screen for non-covalent DNA/ligand interactions, such as DNA intercalation (it increases DNA viscosity), or groove or external binding,[34] which barely affects the DNA viscosity in solution. According to the theory of Cohen and Eisenberg,[35] plotting the cubed root of the relative DNA viscosity $(\eta/\eta_o)^{1/3}$ versus the molar ratio of bound ligand to DNA nucleotide (r), can be used to determine the ligand-binding mode to DNA. If a linear correlation is obtained, slope values close to 0.0 are indicative of groove binding or electrostatic external interactions, whereas positive slope values, reaching values close to 1.0, are representative of classical monointercalant ligands, such as ethidium bromide. Experimentally, some deviations are normally observed, and minor-groove binders slopes can vary within the range from −0.3 to 0.2.[36]

Viscosity assays were conducted at a temperature of 25 ± 0.01 °C by adding small aliquots of each *aldo*-IP to the DNA solutions of *Calf Thymus* (CT) DNA, in 10 mM sodium phosphate buffer (pH 7.2). Flow times were recorded automatically, in the presence (η) and in the absence (η_o) of compounds (**3a–3h**). Viscosity results were plotted as $(\eta/\eta_o)^{1/3}$ versus r, as shown in Fig. 2.

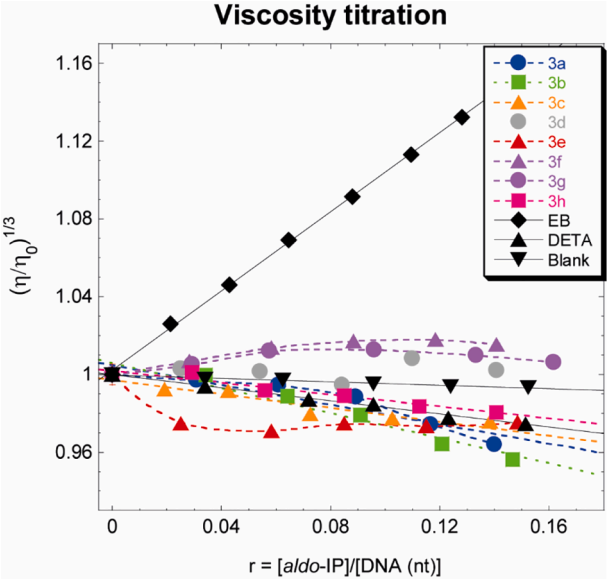

Fig. 2. Viscosity titration experiments of *Calf Thymus* (CT) DNA and *aldo*-IPs **3a–3h** at 25 °C (10 mM sodium phosphate buffer, pH 7.2). Averaged slope values for *aldo*-IPs that show linear correlation are, ca. −0.25 (**3a**), −0.32 (**3b**), −0.18 (**3c**), −0.15 (**3h**). Slopes for selected controls: 1.02 (EB), −0.04 (blank, no compound, dilution effect), −0.17 (DETA). EB: *ethidium bromide (classical intercalant);* DETA*: diethylenetriamine (non-specific, electrostatic binder).*

Among the *aldo*-IPs tested in this work, it was found that derivatives **3a–3c** and **3h** showed a linear $(\eta/\eta o)^{1/3}$ versus r correlation, at the [ligand]/[DNA] ratios used in the experiments. The compounds derived from glucose (**3a**), galactose (**3b**) mannose (**3c**) and ribose (**3h**) were found to produce a slight decrease in DNA viscosity in solution, with their viscosity slopes ranging from −0.32 (**3b**) to −0.15 (**3h**). On the contrary, the compounds derived from xylose and arabinose, **3f** and **3g**, respectively, produced a minor, non-linear viscosity increase. Interestingly, the titration with compound **3d** gave rise to disperse results that did not correlate well linearly but, altogether, they reflect that the compound does not significantly affect the viscosity of CT DNA. Finally, the effect of derivative **3e** also deviated from a linear correlation, first decreasing the DNA viscosity, and then following a similar trend that the one observed with compounds **3a–3c** and **3h**, at higher [ligand]/[DNA] ratios.

Overall, the *aldo*-IPs studied show a behavior consistent with an interaction likely to occur through recognition of the DNA grooves, which may involve a multiple hydrogen bond network in the grooves and/or the phosphate backbone. Our results indicate that the series of *aldo*-IPs do not interact with dsDNA by intercalation through the aromatic imidazophenanthroline ring, as the viscosity slope values determined by this technique are far away from the values accepted for classical intercalation mechanisms, as exemplified by ethidium bromide (Fig. 2).

2.3.3. Equilibrium dialysis

Having established that the *aldo*-APIs altered the viscosity of CT dsDNA upon binding, equilibrium dialysis experiments were carried out next to determine apparent binding association constants. The experiments were adapted from a protocol reported by the Chaires group,[37] which is based on the fundamental thermodynamic principle of equilibrium dialysis and the Crothers competition dialysis method.[38,39]

2 μM solutions of representative *aldo*-IPs **3a**, **3c**, **3d** and **3e** were equilibrated with 75 μM of nucleic acid for 24 h, in the same buffering system used in viscosity titrations. At the end of the equilibration period, SDS (final concentration 1 %) was added to the dialysis solutions, and UV–visible spectra were recorded in order to determine the concentrations of free and DNA-bound ligand. Apparent association constants were calculated by using the equation $K_{app} = C_b/(C_f)(S_{total} - C_b)$,[37c] where C_b is the amount of ligand bound, C_f is the free ligand concentration and $S_{total} = 75$ μM, in monomeric units (base pairs in this case).

Table 5 shows that *aldo*-IPs **3a**, **3c**, **3d** and **3e** bind CT dsDNA, with apparent association constants in the order of 10^4–10^5 M^{-1}. These results are in good agreement with previously reported work. The binding affinity is equivalent to that observed with the *carb*-APIPs[14a] and slightly better than the one reported by Schutte-Smith et al.[7a] with other imidazo [4,5-f][1,10]phenanthroline derivatives, likely explained by the different substitution patterns of the IP scaffold and the presence or not of a carbohydrate motif. Of interest, the relative dsDNA binding affinity of the tested *aldo*-IPs followed a similar trend than in the family of *carb*-APIPs, which, unlike the *aldo*-IP family, was found to significantly increase CT DNA viscosity. It is noteworthy that, in both families of compounds, the lowest dsDNA binding affinity corresponds to deoxysugar derivatives. Further studies will be required to shed light on the molecular mechanisms that account for the biological activity of the *aldo*-IPs.

3. Conclusions

A novel series of carbohydrate-based imidazophenanthroline derivatives was obtained with synthetically useful yields, through a one-pot multistep process, by aerobic oxidative cyclization of 1,10-phenanthroline-5,6-diamine with a selection of unprotected aldoses using $(NH_4)_2SO_4$ as promoter. The experimental results strongly suggest that $(NH_4)_2SO_4$ plays a key role, by promoting the formation of a highly reactive imine intermediate, which should undergo a 6-*exo*-*trig* cyclization to readily generate an amino *N*-glycopyranosylamine, isolated at short reaction times. The formation of the imidazole ring may take place by a favoured 5-*exo*-*tet* cyclization of this derivative, followed by aerobic oxidation of the imidazoline (not detected). All derivatives have shown relevant cytotoxic activity against PC3, HeLa and HT29 tumor cells, with IC_{50} values in the micromolar concentration range. Their cytotoxicity appear to be regulated by both the nature and stereochemistry of the chiral polyhydroxy alkyl chain, having the mannose-based *aldo*-IP the highest activity in the series, substantially better than cisplatin metallodrug in all cell lines tested, and better than G-quadruplex ligand 360A in HeLa and HT29 cells. *Aldo*-IPs **3d**, **3f** and **3h** (obtained from 2-deoxy-D-glucose, xylose and ribose precursors, respectively) were found less toxic than the rest of *aldo*-IPs in healthy human fibroblast cell line HFF1. Moreover, additional experiments of cell cycle analysis and annexin V-PI assay with compounds **3a**, **3c**, **3d** and **3e** revealed that *aldo*-IPs are able to induce apoptosis in HeLa cells, especially compound **3d,** the 2-deoxyglucose derived *aldo*-IP**.** Preliminary DNA interactions have shown that the compounds produce minimal thermal stabilization effects on short oligonucleotide sequences forming duplex or quadruplex secondary structures, mainly affecting the latter. These chiral compounds bind dsDNA through the grooves and/or external binding, discarding a classical intercalation mechanism involving the heteroaromatic part of the conjugate, with association constants in the order of 10^4-10^5 M^{-1}.

4. Experimental

4.1. General methods

All reagents were commercially available (Sigma-Aldrich) in high purity and used as received. The oxidative cyclization reactions were monitored by thin-layer chromatography (TLC) and their composition was determined by ^{1}H NMR spectroscopy; TLC was performed on precoated Kieselgel 60 F_{254} aluminum sheets; plates were eluted with methanol/NH_4OH (30 %) 10:1; detection was first by UV and then by charring with sulfuric acid in ethanol (1:4, v/v). Melting points were taken on an Electrothermal Digital IA9100 apparatus and were uncorrected. Optical rotations were measured in HPLC grade dimethyl sulfoxide on a Perkin-Elmer 341 polarimeter; $[\alpha]_D$ values are given in 10^{-1} deg•cm^2•g^{-1}; concentration is given in mg•mL^{-1}. ESI mass (+mode) spectra were performed on a Thermo Scientific TSQ Quantum LC/MS or an AB Sciex QSTAR Pulsar Q-TOF instruments. IR spectra (KBr disks) were recorded on a FT-IR Perkin-Elmer Spectrum 2000 spectrophotometer. All NMR spectra ^{1}H, ^{13}C, 2D ^{1}H–^{1}H gCOSY, TOCSY, ^{1}H–^{13}C gC2HSQCSE, gHMBC) were recorded on a Varian 300 UNITY-Plus or VNMRS-500 and Brucker-400 spectrometers in $(CD_3)_2SO$ or $(CD_3)_2SO$-D_2O at 298 K using standard pulse sequences. Chemical shifts are reported relative to the residual $(CHD_2)_2SO$ (δ_H 2.50 ppm), or $(CD_3)_2SO$ (δ_C 39.5 ppm); resonance patterns are designated with the notations s

Table 5
Apparent association constants for *aldo*-IPs **3a**, **3c**, **3d** and **3e** obtained by equilibrium dialysis.

	3a (Glucose precursor)	**3c** (Mannose precursor)	**3d** (2-Deoxy-D-glucose precursor)	**3e** (Rhamnose precursor)
DNA	K_{app} (M^{-1}) × 10^{-5}	$K_{app} \times 10^{-5}$	$K_{app} \times 10^{-5}$	$K_{app} \times 10^{-5}$
CT dsDNA	2.68 ± 0.30	1.33 ± 0.13	0.32 ± 0.07	0.63 ± 0.01

(singlet), d (doublet), t (triplet), q (quartet), and m (multiplet); in addition, the notations ap and br are used to indicate an apparent multiplicity and a broad signal; geminal protons at the polyhydroxylated carbon chain resonating at low and high frequency are denoted as H-a and H-b, respectively. Lorentz-Gauss transformation was used to improve the resolution of the ^{1}H NMR spectra. Proton parameters of the polyhydroxy alkyl chain of **3a–h** in $(CD_3)_2SO/D_2O$ were deduced by analysis of the respective spin systems. Errors: ^{1}H, δ ± 0.01 ppm, J ± 0.1 Hz; ^{13}C, δ ± 0.1 ppm.

4.2. Synthesis of 1,10-phenanthroline-5,6-diamine (2)

1,10-Phenanthroline-5,6-diamine (**2**) was synthesized in two steps from 1,10-phenanthroline-5,6-dione[40] by a slight modification of the procedure previously described.[41,42] First, the 1,10-phenanthroline-5,6-dioxime was prepared by treatment of the dione with hydroxylamine-hydrochloride, process that requires a careful control of the reaction and work-up conditions to avoid side reactions.[41d] The reaction was carried out using pyridine as base and solvent as reported for a related system,[42] affording more reproducible results than the use of $CaCO_3$ or Na_2CO_3.[41] A stirred solution of 1,10-phenanthroline-5,6-dione (420 mg, 2 mmol) and hydroxylamine hydrochloride (555 mg, 8 mmol) in 20 mL of pyridine ([dione] = 0.1 M) was heated at 105 °C for 24 h; after cooling to room temperature, water was added and the solid formed was filtered and washed sequentially with water and CH_2Cl_2, and then dried under vacuum to give the 1,10-phenanthroline-5,6-dioxime[41] in a 66 %. Reduction of the dioxime with hydrazine hydrate using Pd/C 10 % as catalyst[41e] at 90 °C for 20 h afforded **2** as a brownish powder (85 %). δ_H (300 MHz; $(CD_3)_2SO$) 5.26 (4H, br s, NH_2), 7.61 (2H, dd, J = 8.5, 4.2 Hz, H-3(8)), 8.49 (2H, dd, J = 8.5, 1.6 Hz, H-4(7)), 8.77 (2H, d, J = 4.2, 1.6 Hz, H-2(9)); δ_C (75 MHz; $(CD_3)_2SO$) 121.9[a] (C-4a(6a)), 122.0 (C-3(8)), 122.7[a] (C-5(6)), 128.5 (C-4(7)), 140.9 (C-10a(10b)), 144.9 (C-2(9)); [a]tentative assignment.

4.3. Synthesis of 2-polyhydroxyalkyl-1H-imidazo[4,5-f][1,10] phenanthrolines (aldo-IPs)

4.3.1. General procedure

A solution of the 1,10-phenantroline-5,6-diamine (210 mg, 1 mmol), the monosaccharide (3 or 5 mmol) and ca. 4 mg of $(NH_4)_2SO_4$ in 30 mL of methanol ([diamine] = 0.033 M) was stirred at 25 or 60 °C for the selected time (Table 1).[14a,b,d] The reaction mixture was then allowed to reach room temperature and the solid obtained was separated by filtration and washed with MeOH and H_2O to remove the $(NH_4)_2SO_4$ salt and to eliminate excess of sugar as well as possible traces of the starting diamine and/or other by-products, and therefore treated with Et_2O. After drying in vacuum, the purity of the derivatives **3a–h** was checked by TLC, ^{1}H NMR and analytical data.

4.3.1.1. (1′S,2′R,3′R,4′R)-2-(1,2,3,4,5-Pentahydroxy)pentyl-1H-imidazo [4,5f][1,10]phenanthroline (3a).

Pale yellow solid; yield: 90 %; Rf = 0.42; mp 275–277 °C (decomposition); $[\alpha]_D^{22}$ + 13 (*c* 1.0 in DMSO); IR (KBr) υ_{max} 3268 br (NH and OH), 1608 (δ NH), 1566, 1504, 1470 (C=N, C=C), 1073, 1042 cm^{-1}, δ_H (500 MHz; $(CD_3)_2SO$-D_2O) 3.34[a] (1H, dd, J = −12.2, 5.7 Hz, H-5′a), 3.36[a] (1H, dd, J = 8.1, 1.9 Hz, H-3′), 3.54[b] (1H, ddd, J = 8.1, 5.7, 3.4 Hz, H-4′), 3.56[b] (1H, dd, J = −12,2, 3.4 Hz, H-5′b), 4.15 (1H, dd, J = 6.4, 1.9 Hz, H-2′), 5.07 (1H, d, J = 6.4 Hz, H-1′), 7.80[c] (2H, dd, J = 8,2, 4.3 Hz, H-5(10)), 8.88[d] (2H, br s, H-4(11)), 8.99 (2H, dd, J = 4.3, 1.8 Hz, H-6(9)); [a,b] partially overlapped signals; [c] 7.79 (2H, m) in $(CD_3)_2SO$; [d] two signals were observed for H-4(11) protons in $(CD_3)_2SO$ at 8.82 (1H, dd, J = 8,0, 1.5 Hz) and 9.01 (1H, ap d, J = 8,0 Hz), partially overlapped with the signal of H-6(9); NH and OH resonances (500 MHz; $(CD_3)_2SO$) 4.30 (1H, ap t, J = 5,7 Hz, OH-5′), 4.51 (1H, d, J = 5,6 Hz, OH-4′), 4.61 (1H, d, J = 6,6 Hz, OH-3′), 4.64 (1H, d, J = 6.4 Hz, OH-2′), 5.85 (1H, d, J = 4.2 Hz, OH-1′), 13.47 (1H, br s, NH); δ_C (125 MHz; $(CD_3)_2SO$) 63.4 (C-5′), 70.2 (C-1′), 71.2 (C-3′), 71.5 (C-4′), 72.0 (C-2′), 119.7[e] (C-3b(11a)), 123.2 (C-5(10)), 123.8[e] (C-3b(11a)), 129.6 (C-4(11)), 143.3 (C-7a(7b)), 147.5 (C-6(9)), 155.2 (C-2); [e]values deduced from ^{1}H–^{13}C gHMBC spectrum, tentative assignment; (C-3a(11b)) beyond detection. HRMS (ESI-TOF): $(M + H)^+$, found 371.1363 (100 %) $C_{18}H_{19}N_4O_5$ requires 371.1350.

4.3.1.2. (1′S,2′R,3′S,4′R)-2-(1,2,3,4,5-Pentahydroxy)pentyl-1H-imidazo [4,5f][1,10]phenanthroline (3b).

Brownish solid; yield: 80 %; Rf = 0.49; mp 288–290 °C (decomposition); $[\alpha]_D^{22}$ + 19 (*c* 1.0 in DMSO); IR (KBr) υ_{max} 3253 br (NH and OH), 1639 (δ NH), 1570, 1500 (C=N, C=C), 1110 cm^{-1}, δ_H (500 MHz; $(CD_3)_2SO$-D_2O) 3.44[a] (1H, dd, J = −10.6, 6.6 Hz, H-5′a), 3.49[a] (1H, dd, J = −10.6, 6.6 Hz, H-5′b), 3.69 (1H, dd, J = 9.4, 1.5 Hz, H-3′), 3.79 (1H, ap td, J = 6,6, 1.5 Hz, H-4′), 3.98 (1H, dd, J = 9.4, 1.7 Hz, H-2′), 5.29 (1H, d, J = 1.7 Hz, H-1′), 7.78 (2H, dd, J = 8,1, 4.3 Hz, H-5(10)), 8.92[b] (2H, br s, H-4(11)), 8.98 (2H, dd, J = 4.3, 2.0 Hz, H-6(9)); [a] partially overlapped signals; [b] two broad singlets were observed for H-4(11) protons in $(CD_3)_2SO$ at 8.81 and 9.04; NH and OH resonances (500 MHz; $(CD_3)_2SO$) 4.27 (1H, d, J = 5,5 Hz, OH-4′), 4.34 (1H, d, J = 7,6 Hz, OH-3′), 4.49 (1H, ap t, J = 4.9 Hz, OH-5′), 4.57 (1H, d, J = 7.1 Hz, OH-2′), 5.65 (1H, br d, J = 5.9 Hz, OH-1′), 13.40 (1H, br s, NH); δ_C (125 MHz; $(CD_3)_2SO$) 62.9 (C-5′), 67.7 (C-1′), 68.9 (C-3′), 69.7 (C-4′), 72.6 (C-2′), 122.9 (C-5(10)), 129.4 (C-4(11)), 143.2 (C-7a(7b)), 147.1 (C-6(9)), 156.4 (C-2); (C-3a(11b)) and (C-3b(11a)) beyond detection. HRMS (ESI-TOF): $(M + H)^+$, found 371.1348 (100 %) $C_{18}H_{19}N_4O_5$ requires 371.1350, $(M + Na)^+$, found 393.1169 (44 %) $C_{18}H_{18}N_4O_5Na$ requires 393.1169.

4.3.1.3. (1′R,2′R,3′R,4′R)-2-(1,2,3,4,5-Pentahydroxy)pentyl-1H-imidazo [4,5f][1,10]phenanthroline (3c).

Pale brownish solid; yield: 92 %; Rf = 0.43; mp 260–262 °C (decomposition); $[\alpha]_D^{22}$−17 (*c* 1.0 in DMSO); IR (KBr) υ_{max} 3215 br (NH and OH), 1614 (δ NH), 1540, 1490 (C=N, C=C), 1080 cm^{-1}, δ_H (500 MHz; $(CD_3)_2SO$-D_2O) 3.46 (1H, dd, J = −11.0, 6.1 Hz, H-5′a), 3.55 (1H, ddd, J = 8.7, 6,1, 3.3 Hz, H-4′), 3.68 (1H, dd, J = −11.0, 3.3 Hz, H-5′b), 3.76 (1H, dd, J = 8.7, 1.0 Hz, H-3′), 4.20 (1H, dd, J = 8.9, 1.0 Hz, H-2′), 4.92 (1H, d, J = 8.9 Hz, H-1′), 7.80 (2H, dd, J = 8,1, 4.3 Hz, H-5(10)), 8.84 (1H, br s, H-4(11)), 8.92 (1H, br s, H-4(11)), 9.00 (2H, dd, J = 4.3, 1.8 Hz, H-6(9)); NH and OH resonances (500 MHz; $(CD_3)_2SO$) 4.38 (1H, ap t, J = 5.7, 5.2 Hz, OH-5′), 4.43 (1H, d, J = 6.8 Hz, OH-2′), 4.47 (1H, d, J = 7,7 Hz, OH-3′), 4.54 (1H, d, J = 5.0 Hz, OH-4′), 5.95 (1H, br d, J = 4.9 Hz, OH-1′), 13.23 (1H, br s, NH); δ_C (75 MHz; $(CD_3)_2SO$) 63.9 (C-5′), 68.1 (C-1′), 69.7 (C-3′), 71.2 (C-4′), 71.6 (C-2′), 119.7[a] (C-3b(11a), 123.4 (C-5(10)), 124.0[a] (C-3b(11a), 129.6 (C-4(11)), 143.3 (C-7a(7b)), 147.6 (C-6(9), 156.4 (C-2); [a]values deduced from ^{1}H–^{13}C gHMBC spectrum, tentative assignment; (C-3a(11b)) beyond detection. HRMS (ESI-TOF): $(M + H)^+$, found 371.1348 (100 %) $C_{18}H_{19}N_4O_5$ requires 371.1350, $(M + Na)^+$, found 393.1169 (40 %) $C_{18}H_{18}N_4O_5Na$ requires 393.1169.

4.3.1.4. (2′R,3′R,4′R)-2-(2,3,4,5-Tetrahydroxy)pentyl-1H-imidazo[4,5f] [1,10]phenanthroline (3d).

Pale yellow powder; yield: 90 %; Rf = 0.54; mp 250–252 °C (decomposition); $[\alpha]_D^{22}$ + 32 (*c* 1.0 in DMSO); IR (KBr) υ_{max} 3218 br (NH and OH), 1619 (δ NH), 1554, 1460 (C=N, C=C), 1060 cm^{-1}, δ_H (500 MHz; $(CD_3)_2SO$-D_2O) 3.12 (1H, dd, J = −14.5, 5.1 Hz, H-1′a), 3.17 (1H, dd, J = −14.5, 8.8 Hz, H-1′b), 3.30 (1H, dd, J = 8.5, 1.4 Hz, H-3′), 3.43 (1H, dd, J = −11.0, 6.0 Hz, H-5′a), 3.55 (1H, ddd, J = 8.5, 6.0, 3.4 Hz, H-4′), 3.63[a] (1H, dd, J = −11.0, 3.4 Hz, H-5′b), 4.35 (1H, ddd, J = 8.8, 5.1, 1.4 Hz, H-2′), 7.80 (2H, dd, J = 8,1, 4.3 Hz, H-5(10)), 8.78 (1H, br s, H-4(11)), 8.80 (1H, br s, H-4(11)), 8.99 (2H, dd, J = 4.3, 1.4 Hz, H-6(9)); [a] partially overlapped with residual H_2O signal; NH and OH resonances (500 MHz; $(CD_3)_2SO$) 4.39 (1H, br s, OH, overlapped with H-2′ signal), 4.58 (3H, br s, OH), 13.27 (1H, br s, NH); δ_C (125 MHz; $(CD_3)_2SO$) 33.5 (C-1′), 63.4 (C-5′), 68.7 (C-2′), 71.0 (C-4′), 72.4 (C-3′), 122.8 (C-5(10)), 128.9 (C-4(11)), 143.3 (C-7a(7b)), 147.0 (C-6(9), 155.4 (C-2); (C-3a(11b)) and (C-3b(11a)) beyond detection. HRMS (ESI-TOF):

$(M + H)^+$, found 355.1398 (100 %) $C_{18}H_{19}N_4O_4$ requires 355.1401, $(M + Na)^+$, found 377.1221 (39 %) $C_{18}H_{18}N_4O_4Na$ requires 377.1220.

*4.3.1.5. (1′S,2′S,3′S,4′S)-2-(1,2,3,4-Tetrahydroxy)pentyl-1H-imidazo [4,5f][1,10]phenanthroline (**3e**).* Pale yellow solid; yield: 67 %; Rf = 0.53; mp 267–269 °C (decomposition); $[\alpha]_D^{22}$ + 12 (*c* 1.0 in DMSO); IR (KBr) υ_{max} 3302 br (NH and OH), 1612 (δ NH), 1520, 1485 (C=N, C=C), 1068 cm^{-1}, δ_H (500 MHz; $(CD_3)_2SO$-D_2O) 1.17 (3H, d, *J* = 6.2 Hz, CH_3-5′a), 3.51 (1H, dd, *J* = 8.3, 1.2 Hz, H-3′), 3.65 (1H, dq, *J* = 8.3, 6.2 Hz, H-4′), 4.21 (1H, dd, *J* = 8.8, 1.2 Hz, H-2′), 4.90 (1H, d, *J* = 8.8 Hz, H-1′), 7.80 (2H, dd, *J* = 8,1, 4.3 Hz, H-5(10)), 8.88[a] (1H, br s, H-4(11)), 8.89[a] (1H, br s, H-4(11)), 8.99 (2H, dd, *J* = 4.3, 1.8 Hz, H-6(9)); [a] 8.89 (2H, br s) in $(CD_3)_2SO$; NH and OH resonances (500 MHz; $(CD_3)_2SO$) 4.36 (1H, br d, *J* = 6.0 Hz, OH), 4.44 (1H, br s, OH), 4.53 (1H, br d, *J* = 4.4 Hz, OH), 5.96 (1H, d, *J* = 5.0 Hz, OH-1′), 13.31 (1H, br s, NH); δ_C (125 MHz; $(CD_3)_2SO$) 20.6 (CH_3-5′), 65.8 (C-4′), 68.0 (C-1′), 71.1 (C-2′), 73.3 (C-3′), 122.9 (C-5(10)), 129.2 (C-4(11)), 143.3 (C-7a(7b)), 147.2 (C-6(9), 156.4 (C-2); (C-3a(11b)) and (C-3b(11a)) beyond detection. HRMS (ESI-TOF): $(M + H)^+$, found 355.1397 (100 %) $C_{18}H_{19}N_4O_4$ requires 355.1401, $(M + Na)^+$, found 377.1222 (11 %) $C_{18}H_{18}N_4O_4Na$ requires 377.1220.

*4.3.1.6. (1′R,2′S,3′S)-2-(1,2,3,4-Tetrahydroxy)butyl-1H-imidazo[4,5f] [1,10]phenanthroline (**3f**).* Yellowish powder; yield: 48 %; Rf = 0.53; mp 230–232 °C (decomposition); $[\alpha]_D^{22}$ − 28 (*c* 1.0 in DMSO); IR (KBr) υ_{max} 3198 br (NH and OH), 1628 (δ NH), 1580, 1475 (C=N, C=C), 1072 cm^{-1}, δ_H (500 MHz; $(CD_3)_2SO$-D_2O) 3.45 (1H, dd, *J* = −10.1, 5.4 Hz, H-4′a), 3.53[a] (2H, m, H-3′, H-4′b), 3.95 (1H, dd, *J* = 5.3, 3.1 Hz, H-2′), 5.08 (1H, d, *J* = 5.3 Hz, H-1′), 7.80 (2H, dd, *J* = 8,1, 4.3 Hz, H-5(10)), 8.84[b] (1H, br s, H-4(11)), 8.93[b] (1H, br s, H-4(11)), 8.99 (2H, dd, *J* = 4.3, 1.7 Hz, H-6(9)); [a] 3.53 (1H, ap dt, *J* = −10.7, 5.3 Hz, H-4′b), 3.58 (1H, m, H-3′) in $(CD_3)_2SO$; [b] two broad singlets were observed for H-4(11) protons in $(CD_3)_2SO$ at 8.53 and 9.01; NH and OH resonances (500 MHz; $(CD_3)_2SO$) 4.55 (1H, ap t, *J* = 5.3 Hz, OH-4′), 4.65 (2H, d, *J* = 5.8 Hz, OH-2′, OH-3′), 5.85 (1H, d, *J* = 4.6 Hz, OH-1′), 13.45 (1H, br s, NH); δ_C (125 MHz; $(CD_3)_2SO$) 62.4 (C-4′), 69.2 (C-1′), 71.7 (C-3′), 72.9 (C-2′), 123.0 (C-5(10)), 129.4 (C-4(11)), 143.3 (C-7a(7b)), 147.3 (C-6(9), 155.7 (C-2); (C-3a(11b)) and (C-3b(11a)) beyond detection. HRMS (ESI-TOF): $(M + H)^+$, found 341.1240 (100 %) $C_{18}H_{19}N_4O_4$ requires 341.1244, $(M + Na)^+$, found 363.1060 (56 %) $C_{18}H_{18}N_4O_4Na$ requires 363.1064.

*4.3.1.7. (1′R,2′S,3′R)-2-(1,2,3,4-Tetrahydroxy)butyl-1H-imidazo[4,5f] [1,10]phenanthroline (**3g**).* Brownish powder; yield: 66 %; Rf = 0.51; mp 241–243 °C (decomposition); $[\alpha]_D^{22}$ − 15 (*c* 1.0 in DMSO); IR (KBr) υ_{max} 3209 br (NH and OH), 1615 (δ NH), 1576, 1481 (C=N, C=C), 1068 cm^{-1}, δ_H (500 MHz; $(CD_3)_2SO$-D_2O) 3.50[a] (1H, H-4′a), 3.67 (2H, m, H-3′, H-4′b), 3.88 (1H, dd, *J* = 8.2, 2.0 Hz, H-2′), 5.28 (1H, d, *J* = 2.0 Hz, H-1′), 7.83 (2H, dd, *J* = 8,2, 4.4 Hz, H-5(10)), 8.98 (2H, br s, H-4(11)), 9.01 (2H, dd, *J* = 4.4, 1.6 Hz, H-6(9)); [a] overlapped with residual H_2O signal; 3.50 (1H, dd, *J* = −11.8, 6.7 Hz) in $(CD_3)_2SO$; NH and OH resonances (500 MHz; $(CD_3)_2SO$) 4.44 (1H, br s, OH), 4.74 (2H, br s, OH), 5.72 (1H, d, *J* = 5.4 Hz, OH-1′), 13.42 (1H, br s, NH); δ_C (125 MHz; $(CD_3)_2SO$) 63.3 (C-4′), 67.8 (C-1′), 70.9 (C-3′), 73.8 (C-2′), 123.3 (C-5(10)), 130.0 (C-4 (11)), 143.3 (C-7a(7b)), 147.0 (C-6(9), 155.9 (C-2); (C-3a(11b)) and (C-3b(11a)) beyond detection. HRMS (ESI-TOF): $(M + H)^+$, found 341.1240 (100 %) $C_{18}H_{19}N_4O_4$ requires 341.1244, $(M + Na)^+$, found 363.1060 (47 %) $C_{18}H_{18}N_4O_4Na$ requires 363.1064.

*4.3.1.8. (1′S,2′S,3′R)-2-(1,2,3,4-Tetrahydroxy)butyl-1H-imidazo[4,5f] [1,10]phenanthroline (**3h**).* Light brownish solid; yield: 79 %; Rf = 0.50; mp 262–264 °C (decomposition); $[\alpha]_D^{22}$ + 14 (*c* 1.0 in DMSO); IR (KBr) υ_{max} 3195 br (NH and OH), 1608 (δ NH), 1564, 1479 (C=N, C=C), 1072 cm^{-1}, δ_H (500 MHz; $(CD_3)_2SO$-D_2O) 3.46 (1H, dd, *J* = −11.1, 6.2 Hz, H-4′a), 3.62[a] (1H, dd, *J* = −11.1, 3.4 Hz, H-4′b), 3.65[a] (1H, m, *J* = 6.7, 6.2, 3.4 Hz, H-3′), 3.93 (1H, dd, *J* = 6.7, 5.2 Hz, H-2′), 5.11 (1H, d, *J* = 5.2 Hz, H-1′), 7.80 (2H, dd, *J* = 8,1, 4.3 Hz, H-5(10)), 8.91[b] (2H, br s, H-4(11)), 9.00 (2H, dd, *J* = 4.3, 1.5 Hz, H-6(9)); [a] partially overlapped signals; [b] two broad singlets were observed for H-4(11) protons in $(CD_3)_2SO$ at 8.83 and 9.00 (partially overlapped with the signal of H-6(9)); NH and OH resonances (500 MHz; $(CD_3)_2SO$) 4.43 (1H, ap t, *J* = 5.5, 5.1 Hz OH-4′), 4.78 (1H, br s, OH-3′), 4.91 (1H, d, *J* = 5.6 Hz, OH-2′), 6.00 (1H, d, *J* = 4.7 Hz, OH-1′), 13.22 (1H, br s, NH); δ_C (125 MHz; $(CD_3)_2SO$) 62.9 (C-4′), 69.5 (C-1′), 72.4 (C-3′), 74.7 (C-2′), 123.1 (C-5(10)), 129.5 (C-4(11)), 143.2 (C-7a(7b)), 147.4 (C-6(9), 155.2 (C-2); (C-3a(11b)) and (C-3b (11a)) beyond detection. HRMS (ESI-TOF): $(M + H)^+$, found 341.1237 (100 %) $C_{18}H_{19}N_4O_4$ requires 341.1244, $(M + Na)^+$, found 363.1059 (47 %) $C_{18}H_{18}N_4O_4Na$ requires 363.1064.

*4.3.1.9. N-(6-Amino-1,10-phenanthrolyn-5-yl)-β-D-glucopyranosylamine (**4a**).* The product was purified by flash chromatography on silica gel using methanol/NH_4OH (30 %) 10:1 as eluent. Yellow solid; yield: 85 %; Rf = 0.40; mp 244–246 °C (decomposition); IR (KBr) υ_{max} 3100 br (NH and OH), 1608 (δ NH), 1566, 1504, 1470 (C=N, C=C), 1110, 1021 cm^{-1}, δ_H (500 MHz; $(CD_3)_2SO$-D_2O) 2.98 (1H, ddd, *J* = 9.0, 5.7, 2.4 Hz, H-5), 3.17 (1H, ap t, *J* = 9.0, 8.7 Hz, H-4), 3.21 (1H, ap t, *J* = 8.7, 8.3 Hz, H-3), 3.35 (1H, ap t, *J* = 8.7, 8.3 Hz, H-2), 3.43 (1H, dd, *J* = −11.5, 5.7 Hz, H-6a), 3.58 (1H, dd, *J* = −11.5, 2.4 Hz, H-6b), 3.97 (1H, d, *J* = 8.7 Hz, H-1), 7.55 (1H, dd, *J* = 8.4, 4.2 Hz, H-8′), 7.70 (1H, dd, *J* = 8.4, 4.2 Hz, H-3′), 8.64 (1H, dd, *J* = 8.4, 1.5 Hz, H-4′), 8.70 (1H, dd, *J* = 4.2, 1.5 Hz, H-9′), 8.78 (1H, dd, *J* = 8,4, 1.5 Hz, H-7′), 8.97 (1H, dd, *J* = 4.2, 1.5 Hz, H-2′); NH and OH resonances (500 MHz; $(CD_3)_2SO$) 4.23 (1H, ap t, *J* = 5,6 Hz, OH-6), 4.84 (1H, d, *J* = 5,1 Hz, OH-3(4)), 4.92 (1H, d, *J* = 9.3 Hz, NH), 4.99 (1H, br s, OH-3(4)), 5.48 (1H, d, *J* = 4.7 Hz, OH-2), 6.02 (2H, s, NH_2); δ_C (100 MHz; $(CD_3)_2SO$) 61.3 (C-6), 70.3 (C-4), 74.0 (C-2), 77.5, 77.7 (C-3, C-5), 91.2 (C-1), 118.4 (C-5′(6′)), 121.9 (C-4′a(6′a)), 122.4, 123.0 (C-3′(8′)), 130.4, 130.6 (C-4′(7′)), 140.4 (C-10′a(10′b)), 144.5 (C-9′), 148.0 (C-2′). HRMS (ESI-TOF): $(M + H)^+$, found 371.1363 (100 %) $C_{18}H_{19}N_4O_5$ requires 371.1350.

4.4. Cell culture and MTT colorimetric assays

Aldo-IPs antitumor activity in cultured cells was tested as previously reported.[14a] Human PC3 (prostate), HeLa (cervix) and HT29 (colorectal) tumor cells were purchased from American Type Culture Collection (ATCC). Cells and culture media were: PC-3 (CRL-1435™, RPMI), HeLa (CCL-2™, DMEM), HT29 (HTB-38™, McCoy's 5a Medium Modified, Catalog No. 30–2007), HFF-1 (SCRC-1041™, DMEM). Culture media were acquired from Sigma: RPMI 1640, DMEM + 10 % FBS (Fetal Bovine Serum) + 10 % antibiotic (penicillin/streptomycin/amphotericin B). Cells were maintained at 37 °C in the presence of 5 % CO_2, renewing culture media three times per week. On the seeding day, when cells reached 80–100 % confluence, cells were trypsinized, centrifuged and the concentration adjusted to the required experiment concentration. Cells were then seeded at a density of ~10,000 cells/well (~8,000 cells/well in the case of HeLa) into 24-well plates and treated with different concentrations of the *aldo*-IPs (typically to cover the 10 nM-100 μM range), from freshly prepared stock solutions in culture media. The experiments were run in triplicate, in a total 0.55 mL well volume. After 72 h incubation (37 °C/5% CO_2), 50 μL of MTT (5 mg/mL) was added followed by incubation for another 4 h. Then, the medium in each well was replaced by DMSO (0.5 mL) and the absorbance in every well assessed at 570 nm in an ELISA plate reader (ELX 800 Biotech Instruments, Spain). Absorbance values were normalized against negative controls (untreated cells or untreated cells with 0.09 % DMSO (Fig. S39), the maximum DMSO percent used at the highest compound concentration, both in triplicate) and the percentage of viable cells versus compound logarithmic concentration was plotted. IC_{50} values were determined through the equation 1/(1 + 10^(m2 * (log(m1) − x))); m1 = 0.000003; m2 = 1 using Kaleidagragh™ (3.52) software.

4.5. Flow cytometry. Cell cycle analysis and apoptosis assay

Flow cytometry experiments were carried out on a MACSQuant® Analyzer 10 Flow Cytometer (Miltenyi Biotech, 9 Bergisch Gladbach, Germany). Exponentially growing HeLa cells were seeded in 6-well plates in DMEM at a density of 2.5×10^5/well, and subjected to compound treatment (*aldo*-IPs or reference compound 360A,[43] either at ½ IC_{50} equivalent concentrations for 72 h, or at a 10 μM concentration for 48 h. Culture media was added in the case of controls of untreated cells. The cells were then washed with PBS and detached with 0.25 % trypsin/0.2 % EDTA, centrifuged at 1500 rpm for 5 min at room temperature and the pellets were mixed with 500 μL of ice-cold 70 % ethanol and then kept at 4 °C for 30 min. After removing the ethanol by centrifugation, the pellets were washed with 2 mL PBS + 2 % BSA and centrifuged again. The supernatants were discarded and 0.5 mL of propidium iodide solution (PI/RNAse, FxCycle™, Invitrogen™ ref. F10797) was added to cell pellets, mixed well and incubated for 15 min at room temperature before flow cytometry analysis. For each sample, 10,000 events were acquired. Results obtained were analyzed with the MacsQuantify 2.13.1 program.

For the apoptosis assay, part of the cells treated for cell cycle analysis cells were harvested by trypsinization, washed with PBS and stained using Annexin-V FITC & PI kit (Invitrogen™ ref. V 13242) according to the manufacturer's instructions. About 10,000 cells were recorded and analyzed by flow cytometry.

4.6. DNA FRET melting assays

DNA FRET melting experiments with labeled dsDNA F10T (5′- FAM – TAT AGC TA TA/Sp18/TA GCT ATA – TAMRA - 3′) and with telomeric quadruplex DNA F21T (5′- FAM – $(GGG\ TTA)_3GGG$ – TAMRA - 3′) were run according to previously reported protocols.[14a] The oligonucleotides were dissolved in BPC grade water to provide 50 μM stock solutions. 0.25 μM solutions of F21T and F10T were then prepared by mixing the DNA stock solution (50 μM), the corresponding 2X buffer and water. These solutions were heated at 90 °C for 7 min and then cooled at 0 °C (F21T) or gradually to room temperature (F10T) for three hours. The solutions were allowed to stand overnight at 4 °C.

Aldo-IPs were dissolved in water, containing a small proportion of DMSO (50 μM stock solution, 0.05 % DMSO). The compounds were tested at a concentration range from 0 to 10 μM using the oligonucleotide sequences F21T and F10T. Each well of the 96-well microplate contained a 50 μL total volume with a 200 nM oligonucleotide concentration in the corresponding buffer pH = 7.3. The buffering system for F21T contained 10 mM potassium chloride, 90 mM lithium chloride and 10 mM lithium cacodylate; the buffer used with F10T contained 100 mM lithium chloride and 10 mM lithium cacodylate.

The experiments were performed on an ABI PRISM® 7000 Sequence Detection System (Applied Biosystems). The melting procedure included a 5-min incubation at 24 °C followed by a temperature ramp at a 1 °C/min rate with fluorescence measurement at every degree up to 95 °C and subsequently a 5-min incubation at 96 °C followed by a temperature ramp at a − 1 °C/min rate with fluorescence measurement at every degree down to 25 °C. The melting curves were obtained as a change in emission of FAM (6-carboxyfluorescein) excited at 492 nm and emitting at 516 nm. Experiments were run at least in duplicate. The melting temperatures (T_m) were determined from normalized curves as the mid-transition $T_{1/2}$ temperatures. $T_{1/2}$ represents an apparent melting temperature, defined as the temperature where the normalized fluorescence has a value of 0.5.

4.7. Viscosity titrations

The viscosity measurements were performed in a Visco System AVS 470 at 25 °C, using a microUbbelohde (K = 0.01) capillary viscometer.[14a] Solutions of DNA (Calf thymus, CT) and *aldo*-IPs, were prepared in sodium phosphate buffer (10 mM, pH = 7.2). DNA solutions (0.30–0.35 mM, in nucleotides) were equilibrated for 20 min at 25 °C and then 20 flow times were registered. Small aliquots (ca. 20–40 μL) of solutions of the *aldo*-IP (~1.6–1.7 mM) were added next. Before each flow time registration, the solutions were equilibrated for at least 20 min at 25 °C and then 20 flow times were measured. With the averaged flow times and the viscometer constant, the viscosities (μ) for each point were calculated, with μ_o representing the DNA solution viscosity in the absence of compound. The viscosity results were then plotted as $(\mu/\mu_o)^{1/3}$ versus the molar ratio of bound ligand to DNA nt (r).

4.8. Equilibrium dialysis

Experiments were performed as previously reported.[14a] Duplex DNA from calf thymus (CT DNA, deoxyribonucleic acid, activated, type XV), was acquired from Sigma Aldrich and used as provided. A 10 mM sodium phosphate buffer (pH = 7.2) was used, in the same conditions as used in viscosity titrations. For each dialysis assay, a 0.2 mL volume of CT DNA in buffer (75 μM in base pairs) was pipetted into individual dialysis units (Biotech Regenerated Cellulose (RC) membrane, part number 133192, Spectrum Laboratories, Inc.). The dialysis units were then placed in a beaker containing 200 mL of a 2 μM solution of compound in buffer. The beaker was covered with Parafilm and wrapped in aluminum foil, and its contents were allowed to equilibrate with continuous stirring for 24 h at room temperature (22 °C). At the end of the equilibration period, the DNA solutions inside the dialysis units were carefully transferred into microcentrifuge tubes and a 10.0 % (w/v) stock solution of SDS detergent was added to give a final concentration of 1.0 % (w/v). These solutions were allowed to equilibrate for another 2 h, after which the total concentration of the ligand (Ct) was determined by UV–visible absorbance measurements using the extinction coefficients of free *aldo*-IPs calculated in the presence of 1.0 % SDS. The concentration of free compound (C_f) was also established spectrophotometrically using an aliquot of their dialysate solution. The amount of DNA-bound compound (C_b) was then calculated by the difference $C_b = C_t - C_f$ and apparent association constants (K_{app}) determined.

Declaration of competing interest

The authors declare that they have no known competing financial interests or personal relationships that could have appeared to influence the work reported in this paper.

Data availability

Data will be made available on request.

Acknowledgments

The research reported in this work has received funding from Agencia Estatal de Investigación, Spanish MICINN and MINECO (grants PID2019-108251RB-I00/AEI/10.13039/501100011033, CTQ2015-72625-EXP/AEI), and Universidad de Alcalá (UAH, Projects CCG2015/EXP-013, PIUAH22/CC-028, and UAH-AE-2017-2). A.G.-B. is grateful to UAH as a recipient of an Ayuda de Iniciación a la Actividad Investigadora fellowship and to Consejería de Educación, Juventud y Deporte de la Comunidad de Madrid and Fondo Social Europeo (YEI, contract PEJ-2021-AI/BMD-23272). We thank A. Abengózar for his contribution to the synthesis of some reported derivatives. Technical assistance with cell assays by Isabel Trabado, from Unidad de Cultivos UAH (CAI Medicina-Biología), is gratefully acknowledged.

Appendix A. Supplementary material

Supplementary data to this article can be found online at https://doi.org/10.1016/j.bmc.2023.117563.

References

1. (a) Hassan RA, Hamed MIA, Abdou AM, El-Dash Y. Novel antiproliferative agents bearing substituted thieno[2,3-d]pyrimidine scaffold as dual VEGFR-2 and BRAF kinases inhibitors and apoptosis inducers; design, synthesis and molecular docking. *Bioorg Chem*. 2022;125, 105861. https://doi.org/10.1016/j.bioorg.2022.105861. (b) Jamroskovic J, Doimo M, Chand K, et al. Quinazoline ligands induce cancer cell death through selective STAT3 inhibition and G-quadruplex stabilization. *J Am Chem Soc*. 2020;142:2876–2888. https://doi.org/10.1021/jacs.9b11232.(c) Doria F, Pirota V, Petenzi M, Teulade M, et al. Oxadiazole/pyridine-based ligands: a Structural tuning for enhancing G-quadruplex binding. *Molecules*. 2018;23, 2162. https://doi.org/10.3390/molecules23092162.(d) Nguyen TQN, Lim KW, Phan AT. A dual-specific targeting approach based on the simultaneous recognition of duplex and quadruplex motifs. *Sci Rep*. 2017;7, 11969. https://doi.org/10.1038/s41598-017-10583-9.
2. (a) Heravi MM, Zadsirjan V. Prescribed drugs containing nitrogen heterocycles: an overview. *RSC Adv*. 2020;10:44247–44311. https://doi.org/10.1039/d0ra09198g. (b) Taylor AP, Robinson RP, Fobian YM, Blakemore DC, Jones LH, Fadeyi O. Modern advances in heterocyclic chemistry in drug discovery. *Org Biomol Chem*. 2016;14:6611–6637. https://doi.org/10.1039/C6OB00936K.
3. (a) Kumari P, Narayana C, Tiwari G, Sagar R. Chapter Eleven - Glycohybrid molecules in medicinal chemistry: present status and future prospective. In: Tiwari VK, ed. *Carbohydrates in drug discovery and development*. Elsevier; 2020: 451–479. https://doi.org/10.1016/B978-0-12-816675-8.00011-7.(b) Fu J, Wu Z, Zhang L. Clinical applications of the naturally occurring or synthetic glycosylated low molecular weight drugs, in glycans and glycosaminoglycans as clinical biomarkers and therapeutics - part B. In: Zhang L, ed. *Progress in molecular biology and translational science*Vol. 163.(c) Valverde P, Ardá A, Reichardt NC, Jiménez-Barbero J, Gimeno A. Glycans in drug discovery. *Medchemcomm*. 2019;10: 1678–1691. https://doi.org/10.1039/c9md00292h.(d) Pastuch-Gawołek G, Malarz K, Mrozek-Wilczkiewicz A, et al. Small molecule glycoconjugates with anticancer activity. *Eur J Med Chem*. 2016;112:130–144. https://doi.org/10.1016/j.ejmech.2016.01.061.
4. (a) Kappler K, Hennet T. Emergence and significance of carbohydrate-specific antibodies. *Genes Immun*. 2020;21:224–239. https://doi.org/10.1038/s41435-020-0105-9.(b) Sun X, Stefanetti G, Bertid F, Kaspera DL. Polysaccharide structure dictates mechanism of adaptive immune response to glycoconjugate vaccines. *PNAS*. 2019;116:193–198. https://doi.org/10.1073/pnas.1816401115.(c) Varki A. Biological roles of glycans. *Glycobiology*. 2017;27:3–47. https://doi.org/10.1093/glycob/cww086.
5. (a) Teli P, Sahiba N, Sethiya A, Soni J, Agarwal S. Chapter 4 -Imidazole derivatives: Impact and prospects in antiviral drug discovery in heterocyclic drug discovery. In: Agarwal S, ed. *Imidazole-based drug discovery*. Elsevier; 2022:167–193. https://doi.org/10.1016/B978-0-323-85479-5.00001-0.(b) Chopra PN, Sahu JK. Biological significance of imidazole-based analogues in new drug development. *Curr Drug Discov Technol*. 2020;17:574–584. https://doi.org/10.2174/1570163816666190320123340.(c) Rossi R, Ciofalo M. An updated review on the synthesis and antibacterial activity of molecular hybrids and conjugates bearing imidazole moiety. *Molecules*. 2020;25:5133. https://doi.org/10.3390/molecules25215133.(d) Daraji DG, Prajapati NP, Patel HD. Synthesis and applications of 2-substituted imidazole and its derivatives: a review. *J Heterocyclic Chem*. 2019;56:2299–2317. https://doi.org/10.1002/jhet.3641.
6. (a) . In: Marinescu M, ed. *Chemistry and applications of benzimidazole and its derivatives*. London: IntechOpen; 2019. https://doi.org/10.5772/intechopen.81426. (b) Tahlan S, Kumar S, Kakkar S, Narasimhan B. Benzimidazole scaffolds as promising antiproliferative agents: a review. *BMC Chem*. 2019;13:66. https://doi.org/10.1186/s13065-019-0579-6.
7. (a) Kapp LE, Schutte-Smith M, Twigge L, Visse HG. Synthesis, characterization and DNA binding of four imidazo[4,5-f]1,10-phenanthroline derivatives. *J Mol Struct*. 2022;1247, 131235. https://doi.org/10.1016/j.molstruc.2021.131235.(b) Hu S, Ma W, Wang J, et al. Synthesis and anticancer evaluations of novel 1H-imidazole [4,5-f][1,10] phenanthroline derivative for the treatment of colorectal cancer. *Eur J Pharmacol*. 2022;928, 175120. https://doi.org/10.1016/j.ejphar.2022.175120.(c) Hu S, Ma W, Wang J, et al. Synthesis and biological activity of 1H-imidazo[4,5-f][1,10]phenanthroline as a potential antitumor agent with PI3K/AKT/mTOR signaling. *Eur J Pharmacol*. 2022;915, 174514. https://doi.org/10.1016/j.ejphar.2021.174514.(d) Bai M-J, Liu N-Z, Zhou Y–L, et al. Synthesis of fluorinated imidazole[4,5f][1,10] phenanthroline derivatives as potential inhibitors of liver cancer cell proliferation by inducing apoptosis via DNA damage. *ChemMedChem*. 2022;17, e202100537. https://doi.org/10.1002/cmdc.202100537.(e) Fan H, Wang L, Wang X. Synthesis and fluorescent properties of coumarin-benzimidazole and coumarin–phenanthroimidazole hybrids. *J Chem Res*. 2020;44:9–13. https://doi.org/10.1177/1747519819882229.(f) Thakare SS, Chakraborty G, Kothavale S, Mula S, Ray AK, Sekar N. Proton induced modulation of ICT and PET processes in an imidazo-phenanthroline based BODIPY fluorophores. *J Fluoresc*. 2017;27: 2313–2322. https://doi.org/10.1007/s10895-017-2173-4.(g) Pan Y-L, Cai Z-B, Bai L, Ma F-F, Li S-L, Tian Y-P. Green synthesis and photophysical properties of novel 1 H-imidazo[4,5-f][1,10]phenanthroline derivatives with blue/cyan two-photon excited fluorescence. *Tetrahedron*. 2017;73:2886–2893. https://doi.org/10.1016/j.tet.2017.03.075.(h) Yoldas A, Algi F. An imidazo-phenanthroline scaffold enables both chromogenic Fe(II) and fluorogenic Zn(II) detection. *RSC Adv*. 2015;5: 7868–7873. https://doi.org/10.1039/C4RA14182B.
8. (a) Anthony EJ, Bolitho EM, Bridgewater HE, et al. Metallodrugs are unique: opportunities and challenges of discovery and development. *Chem Sci*. 2020;11: 12888–12917. https://doi.org/10.1039/D0SC04082G.(b) Bergamo A, Dyson PJ, Sava G. The mechanism of tumour cell death by metal-based anticancer drugs is not only a matter of DNA interactions, Coordin. *Chem Rev*. 2018;360:17–33. https://doi.org/10.1016/j.ccr.2018.01.009.
9. (a) Kar B, Das U, De SD, et al. GSH-resistant and highly cytoselective ruthenium(ii)-p-cymene-(imidazo[4,5-f][1,10]phenanthrolin-2-yl)phenol complexes as potential anticancer agents. *Dalton Trans*. 2021;50:10369–10373. https://doi.org/10.1039/D1DT01604K.(b) De S, Kumar RS, Gauthaman A, et al. Luminescent ruthenium(II)-para-cymene complexes of aryl substituted imidazo-1,10-phenanthroline as anticancer agents and the effect of remote substituents on cytotoxic activities. *Inorg Chim Acta*. 2021;515, 120066. https://doi.org/10.1016/j.ica.2020.120066.(c) Mondal A, Paira P. Hypoxia efficient and glutathione-resistant cytoselective ruthenium(ii)-p-cymene-arylimidazophenanthroline complexes: biomolecular interaction and live cell imaging. *Dalton Trans*. 2020;49:12865–12878. https://doi.org/10.1039/D0DT02069A.(d) Tokarev SD, Fedorov YV. Ruthenium(II) complexes of 1H-imidazo[4,5-f][1,10] phenanthroline derivatives: physicochemical properties and photosensitizing ability. *INEOS OPEN*. 2020;3:55–65. https://doi.org/10.32931/io2010r.(e) Alexander C, Nithyakumar A, Paul MWB, Samy NA. Platinum(II) complexes of imidazophenanthroline-based polypyridine ligands as potential anticancer agents: synthesis, characterization, in vitro cytotoxicity studies and a comparative ab initio, and DFT studies with cisplatin, carboplatin, and oxaliplatin. *J Biol Inorg Chem*. 2018;23:833–848. https://doi.org/10.1007/s00775-018-1579-z.(f) Schmid M-A, Rentschler M, Frey W, Tschierlei S, Karnahl M. Imidazo-phenanthroline ligands as a convenient modular platform for the preparation of heteroleptic Cu(I) photosensitizers. *Inorganics*. 2018;6, 134. https://doi.org/10.3390/inorganics6040134.(g) Wang Y-C, Qian C, Peng Z-L, et al. Dual topoisomerase I and II poisoning by chiral Ru(II) complexes containing 2-thiophenyl imidazo [4,5-f][1,10] phenanthroline derivatives. *J Inorg Biochem*. 2014;130:15–27. https://doi.org/10.1016/j.jinorgbio.2013.09.015.(h) Stephenson M, Reichardt C, Pinto M, et al. Ru(II) dyads derived from 2-(1-Pyrenyl)-1H-imidazo[4,5-f][1,10] phenanthroline: versatile photosensitizers for photodynamic applications. *J Phys Chem A*. 2014;118:10507–10521. https://doi.org/10.1021/jp504330s.(i) Cardinaels T, Ramaekers J, Nockemann P, et al. Imidazo[4,5-f]-1,10-phenanthrolines: versatile ligands for the design of metallomesogens. *Chem Mater*. 2008;20:1278–1291. https://doi.org/10.1021/cm070637i.
10. (a) García-Quiroz J, Cárdenas-Ochoa N, García-Becerra R, et al. Antitumoral effects of dovitinib in triple-negative breast cancer are synergized by calcitriol in vivo and in vitro. *J Steroid Biochem Mol Biol*. 2021;214, 105979. https://doi.org/10.1016/j.jsbmb.2021.105979.(b) Ferguson F, Gray N. Kinase inhibitors: the road ahead. *Nat Rev Drug Discov*. 2018;17:353–377. https://doi.org/10.1038/nrd.2018.21.(c) Hasinoff BB, Wu X, Nitiss JL, Kanagasabai R, Yalowich JC. The anticancer multi-kinase inhibitor Dovitinib also targets topoisomerase I and topoisomerase II. *Biochem Pharmacol*. 2012;84:1617–1626. https://doi.org/10.1016/j.bcp.2012.09.023.
11. (a) Kosiol N, Juranek S, Brossart P, Heine A, Paeschke K. G-quadruplexes: a promising target for cancer therapy. *Mol Cancer*. 2021;20:40. https://doi.org/10.1186/s12943-021-01328-4.(b) Varshney D, Spiegel J, Zyner K, Tannahill D, Balasubramanian S. The regulation and functions of DNA and RNA G-quadruplexes. *Nat Rev Mol Cell Biol*. 2020;21:459–474. https://doi.org/10.1038/s41580-020-0236-x.(c) Tan J, Lan L. The DNA secondary structures at telomeres and genome instability. *Cell Biosci*. 2020;10:47. https://doi.org/10.1186/s13578-020-00409-z. (d) Mukherjee AK, Sharma S, Chowdhury S. Non-duplex G-quadruplex structures emerge as mediators of epigenetic modifications. *Trends Genet*. 2019;35:129–135. https://doi.org/10.1016/j.tig.2018.11.001.(e) O'Hagan MP, Morales JC, Galan MC. Binding and beyond: what else can G-quadruplex ligands do? *Eur J Org Chem*. 2019:4995–5017. https://doi.org/10.1002/ejoc.201900692.
12. (a) Mendes E, Aljnadi IM, Bahls B, Victor BL, Paulo A. Major achievements in the design of quadruplex-interactive small molecules. *Pharmaceuticals (Basel)*. 2022;15: 300. https://doi.org/10.3390/ph15030300.(b) Paul R, Dutta D, Das T, Debnath M, Dash J. G4 sensing pyridyl-thiazole polyamide represses c-KIT expression in leukemia cells. *Chem Eur J*. 2021;27:8590–8599. https://doi.org/10.1002/chem.202100907.(c) Sengupta A, Ganguly A, Chowdhury S. Promise of G-quadruplex structure binding ligands as epigenetic modifiers with anti-cancer effects. *Molecules*. 2019;24:582. https://doi.org/10.3390/molecules24030582.(d) Chilka P, Desai N, Datta B. Small molecule fluorescent probes for G-quadruplex visualization as potential cancer theranostic agents. *Molecules*. 2019;24:752. https://doi.org/10.3390/molecules24040752.(e) Pirota V, Nadai M, Doria F, Richter SN. Naphthalene diimides as multimodal G-quadruplex-selective ligands. *Molecules*. 2019;24:426. https://doi.org/10.3390/molecules24030426.(f) Yu Z, Fenk KD, Huang D, Sen S, Cowan JA. Rapid telomere reduction in cancer cells induced by G–quadruplex-targeting copper complexes. *J Med Chem*. 2019;62:5040–5048. https://doi.org/10.1021/acs.jmedchem.9b00215.(g) Rigo R, Palumbo M, Sissi C. G-quadruplexes in human promoters: a challenge for therapeutic applications. *Biochim Biophys Acta*. 2017;1861(5 Pt B):1399–1413. https://doi.org/10.1016/j.bbagen.2016.12.024.(h) Neidle S. Quadruplex nucleic acids as targets for anticancer therapeutics. *Nat Rev Chem*. 2017;1:41. https://doi.org/10.1038/s41570-017-0041.
13. (a) Arévalo-Ruiz M, Amrane S, Rosu F, et al. Symmetric and dissymmetric carbohydrate-phenyl ditriazole derivatives as DNA G-quadruplex ligands: synthesis, biophysical studies and antiproliferative activity. *Bioorg Chem*. 2020;99, 103786. https://doi.org/10.1016/j.bioorg.2020.103786.(b) Arévalo-Ruiz M, Doria F, Belmonte-Reche E, et al. Synthesis, binding properties, and differences in cell uptake of G-quadruplex ligands based on carbohydrate naphthalene diimide conjugates. *Chem Eur J*. 2017;23:2157–2164. https://doi.org/10.1002/chem.201604886.(c) Street STG, Chin DN, Hollingworth GJ, Berry M, Morales JC, Galan MC. Divalent naphthalene diimide ligands display high selectivity for the human telomeric G-quadruplex in K+ buffer. *Chem Eur J*. 2017;23:6953–6958. https://doi.org/10.1002/chem.201700140.(d) Gómez-Pinto I, Vengut-Climent E, Lucas R, et al.

Carbohydrate–DNA interactions at G-quadruplexes: folding and stability changes by attaching sugars at the 5′-end. *Chem Eur J*. 2013;19:1920–1927. https://doi.org/10.1002/chem.201203902.

14. (a) Gratal P, Arias-Pérez M-S, Gude L. 1H-imidazo[4,5-f][1,10]phenanthroline carbohydrate conjugates: synthesis, DNA interactions and cytotoxic activity. *Bioorg Chem*. 2022;125, 105851. https://doi.org/10.1016/j.bioorg.2022.105851.(b) Jäger S, Gude L, Arias-Pérez MS. 4,5-Diazafluorene N-glycopyranosyl hydrazones as scaffolds for potential bioactive metallo-organic compounds: synthesis, structural study and cytotoxic activity. *Bioorg Chem*. 2018;81:405–413. https://doi.org/10.1016/j.bioorg.2018.08.019.(c) Duskova K, Sierra S, Arias-Pérez MS, Gude L. Human telomeric G-quadruplex DNA interactions of N-phenanthroline glycosylamine copper(II) complexes. *Bioorg Med Chem*. 2016;24:33–41. https://doi.org/10.1016/j.bmc.2015.11.037.(d) Duskova K, Gude L, Arias-Pérez MS. N-Phenanthroline glycosylamines: synthesis and copper(II) complexes. *Tetrahedron*. 2014;70:1071–1076. https://doi.org/10.1016/j.tet.2013.12.044.
15. (a) Ramu V, Gautam S, Garai A, Kondaiah P, Chakravarty AR. Glucose-appended platinum(II)-BODIPY conjugates for targeted photodynamic therapy in red light. *Inorg. Chem.* 2018;57:1717–1726. https://doi.org/10.1021/acs.inorchem.7b02249. (b) Ma J, Yang X, Hao W, Huang Z, Wang X, Wang PG. Mono-functionalized glycosylated platinum(IV) complexes possessed both pH and redox dual-responsive properties: exhibited enhanced safety and preferentially accumulated in cancer cells in vitro and in vivo. *Eur. J. Med. Chem.* 2017;128:45–55. https://doi.org/10.1016/j.ejmech.2017.01.032.(c) Mikata Y, Gottschaldt M. Metal complexes of carbohydrate-targeted ligands. In: Storr T, ed. *Medicinal Inorganic Chemistry in Ligand Design in Medicinal Inorganic Chemistry*. Chichester: Wiley & Sons; 2014:145–174. (d) Banik B, Somyajit K, Hussain A, Nagaraju G, Chakravarty AR. Carbohydrate-appended photocytotoxic (imidazophenanthroline)-oxovanadium(IV) complexes for cellular targeting and imaging. *Dalton Trans.* 2014;43:1321–1331. https://doi.org/10.1039/C3DT52087K.
16. (a) Harland A, Liu X, Ghirardello M, Galan MC, Perks CM, Kurian KM. Glioma stem-like cells and metabolism: potential for novel therapeutic strategies. *Front Oncol*. 2021;11, 743814. https://doi.org/10.3389/fonc.2021.743814.(b) Granchi C, Fortunato S, Minutolo F. Anticancer agents interacting with membrane glucose transporters. *MedChemComm*. 2016;7:1716–1729. https://doi.org/10.1039/C6MD00287K.(c) Zhang D, Li J, Wang F, Hu J, Wang S, Sun Y. 2-Deoxy-D-glucose targeting of glucose metabolism in cancer cells as a potential therapy. *Cancer Lett*. 2014;355:176–183. https://doi.org/10.1016/j.canlet.2014.09.003.
17. (a) Paul A, Zhang B-D, Mohapatra S, et al. Novel mannitol-based small molecules for inhibiting aggregation of α-synuclein amyloids in Parkinson's disease. *Front Mol Biosci*. 2019;22:16. https://doi.org/10.3389/fmolb.2019.00016.(b) Dias CJ, Sardo I, Moura NMM, et al. An efficient synthetic access to new uracil-alditols bearing a porphyrin unit and biological assessment in prostate cancer cells. *Dyes Pigm*. 2019;173, 107996. https://doi.org/10.1016/j.dyepig.2019.107996.(c) Chang Y, Hsu W-H, Yang W-B, et al. Structure-activity relationship of three synthesized benzimidazole-based oligosaccharides in human platelet activation. *Int J Mol Med*. 2017;40:1520–1528. https://doi.org/10.3892/ijmm.2017.3133.(d) Khalafi-Nezhad A, Nourisefata M, Panahi F. Carbohydrates as reagent in multicomponent reaction: one-pot access to a new library of hydrophilic substituted pyrimidine-fused heterocycles. *Org Biomol Chem*. 2014;12:9419–9426. https://doi.org/10.1039/C4OB01791A.(e) Peterson KE, Cinelli MA, Morrell AE, et al. Alcohol-, diol-, and carbohydrate-substituted indenoisoquinolines as topoisomerase I inhibitors: investigating the relationships involving stereochemistry, hydrogen bonding, and biological activity. *J Med Chem*. 2011;54:4937–4953. https://doi.org/10.1021/jm101338z.
18. (a) Lin C, Hung W-T, Kuo C-Y, Liao K-S, Liu Y-C, Yang W-B. I2-catalyzed oxidative condensation of aldoses with diamines: synthesis of aldo-naphthimidazoles for carbohydrate analysis. *Molecules*. 2010;15:1340–1353. https://doi.org/10.3390/molecules15031340.(b) Lin C, Lai P-T, Liao S-K-S, Hung W-T, Yang W-B, Fang J-M. Using molecular iodine in direct oxidative condensation of aldoses with diamines: an improved synthesis of aldo-benzimidazoles and aldo-naphthimidazoles for carbohydrate analysis. *J Org Chem*. 2008;73:3848–3853. https://doi.org/10.1021/jo800234x.
19. (a) Lang S, Huang X. Carbohydrate conjugates in vaccine developments. *Front Chem*. 2020;8:284. https://doi.org/10.3389/fchem.2020.00284.(b) Mettu R, Chen C-Y, Wu C-Y. Synthetic carbohydrate-based vaccines: challenges and opportunities. *J Biomed Sci*. 2020;27:9. https://doi.org/10.1186/s12929-019-0591-0.(c) Shelton J, Lu X, Hollenbaugh JA, Cho JH, Amblard F, Schinazi RF. Metabolism, biochemical actions, and chemical synthesis of anticancer nucleosides, nucleotides, and base analogs. *Chem Rev*. 2016;116:14379–21445. https://doi.org/10.1021/acs.chemrev.6b00209.(d) Weber GF. *Molecular Therapies of Cancer*. Heidelberg: Springer; 2015.(e) Chabre YM, Roy R. Design and creativity in synthesis of multivalent neoglycoconjugates. *Adv Carbohydr Chem Biochem*. 2010;63:165–393. https://doi.org/10.1016/s0065-2318(10)63006-5.
20. (a) Beigel JH, Tomashek KM, Dodd LE, et al. Remdesivir for the treatment of Covid-19 - final report. *N Engl J Med*. 2020;383:1813–1826. https://doi.org/10.1056/NEJMoa2007764.(b) Berdis AJ. Inhibiting DNA Polymerases as a therapeutic intervention against cancer. *Front Mol Biosci*. 2017;4:78. https://doi.org/10.3389/fmolb.2017.00078.
21. (a) Maier FC, Schweifer A, Damaraju VL, et al. 2-Nitroimidazole-furanoside derivatives for hypoxia imaging—investigation of nucleoside transporter interaction, 18F-labeling and preclinical PET imaging. *Pharmaceuticals*. 2019;12:31. https://doi.org/10.3390/ph12010031.(b) Kumar P, Roselt P, Reischl G, et al. β-[18F]fluoro azomycin arabinoside (β -[18F]FAZA): synthesis, radiofluorination and preliminary PET imaging of murine A431 tumors. *Curr Radiopharm*. 2017;10:93–101. https://doi.org/10.2174/1874471010666170313120540.
22. (a) Street STG, Peñalver P, O'Hagan MP, Hollingworth GJ, Morales JC, Galan MC. Imide condensation as a strategy for the synthesis of core-diversified G-quadruplex ligands with anticancer and antiparasitic activity. *Chem Eur J*. 2021;27:7712–7721. https://doi.org/10.1002/chem.202100040.(b) Pont I, Martínez-Camarena I, Galiana-Rosellj C, et al. Development of polyamine-substituted triphenylamine ligands with high affinity and selectivity for G-quadruplex DNA. *ChemBioChem*. 2020;21:1167–1177. https://doi.org/10.1002/cbic.201900678.(c) Lic G, Tanga H, Liua C, et al. One-step synthesis of methylene-bridged bis-carbazole and evaluation of its antitumor activity and G-quadruplex DNA binding property. *Bioorg. Chem.* 2019;90:10307. https://doi.org/10.1016/j.bioorg.2019.103074.
23. Eggersdorfer M, Laudert D, Létinois U, et al. One hundred years of vitamins-A success story of the natural sciences. *Angew Chem Int Ed*. 2012;51:12960–12990. https://doi.org/10.1002/anie.201205886.
24. Lee Y-S, Cho Y-H, Lee S, et al. Significant facilitation of metal-free aerobic oxidative cyclization of imines with water in synthesis of benzimidazoles. *Tetrahedron*. 2015;71:532–538. https://doi.org/10.1016/j.tet.2014.12.043.
25. (a) Chen G-F, Li H-Y, Xiao N, et al. Efficient synthesis of 2-imidazolines in the presence of molecular iodine under ultrasound irradiation. *Aust J Chem*. 2014;67:1516–1521. https://doi.org/10.1071/CH13700.(b) Yadav TB, Singh V. Iodine promoted simple synthesis of benzimidazole acylclonucleosides. *Indian J Chem*. 2013;52B:1536–1539.(c) Ishihara M, Togo H. Direct oxidative conversion of aldehydes and alcohols to 2-imidazolines and 2-oxazolines using molecular iodine. *Tetrahedron*. 2007;63:1474–1480. https://doi.org/10.1016/j.tet.2006.11.077.(d) Gogoi P, Konwar D. An efficient and one-pot synthesis of imidazolines and benzimidazoles via anaerobic oxidation of carbon–nitrogen bonds in water. *Tetrahedron Lett*. 2006;47:79–82. https://doi.org/10.1016/j.tetlet.2005.10.134.(e) Togo H, Iida S. Synthetic use of molecular iodine for organic synthesis. *Synlett*. 2006:2159–2175. https://doi.org/10.1055/s-2006-950405.
26. (a) Feizpour F, Jafarpour M, Rezaeifar A. A tandem synthesis of benzimidazoles by cobalt ascorbic acid complex coated on TiO2 nanoparticles under visible light. *Catal Lett*. 2018;148:30–40. https://doi.org/10.1007/s10562-017-2232-0.(b) Rostamizadeh S, Aryan R, Ghaien HR. Aqueous 1 M glucose solution as a novel and fully green reaction medium and catalyst for the oxidant-free synthesis of 2-arylbenzimidazoles. *Synth Commun*. 2011;41:1794–1804. https://doi.org/10.1080/00397911.2010.492460.(c) Ruiz VR, Corma A, Sabater MJ. New route for the synthesis of benzimidazoles by a one-pot multistep process with mono and bifunctional solid catalysts. *Tetrahedron*. 2010;66:730–735. https://doi.org/10.1016/j.tet.2009.11.048.
27. Das TM, Rao CP, Kolehmainen E. Synthesis and characterisation of N-glycosyl amines from the reaction between 4,6-O-benzylidene-D-glucopyranose and substituted aromatic amines and also between 2-(o-aminophenyl)benzimidazole and pentoses or hexoses Carbohydr. *Carbohydr Res*. 2001;334:261–269. https://doi.org/10.1016/S0008-6215(01)00202-6.
28. Alabugin IV, Gilmore K. Finding the right path: Baldwin "Rules for Ring Closure" and stereoelectronic control of cyclizations. *Chem Commun*. 2013;49:11246–11250. https://doi.org/10.1039/C3CC43872D.
29. (a) Su F, Sun Z, Su W, Liang X. NMR investigation and theoretical calculations on the tautomerism of benzimidazole compounds 2018. *J Mol Struct*. 2018;1173:690–696. https://doi.org/10.1016/j.molstruc.2018.07.038.(b) Nieto CI, Cabildo P, García MA, Claramunt RM, Alkorta I, Elguero J. An experimental and theoretical NMR study of NH-benzimidazoles in solution and in the solid state: proton transfer and tautomerism. *Beilstein J Org Chem*. 2014;10:1620–1629. https://doi.org/10.3762/bjoc.10.168.
30. (a) Mattsson I, Sitdikov R, Gunell ACM, Lahtinen M, Saloranta-Simella T, Leino R. Improved synthesis and application of conjugation-amenable polyols from D-mannose. *RSC Adv*. 2020;10:3960–3966. https://doi.org/10.1039/c9ra10378c.(b) Mattsson I, Lahtinen M, Peuronen A, et al. Thermal, spectroscopic, and crystallographic analysis of mannose-derived linear polyols. *Cryst Growth Des*. 2018;18:3151–3160. https://doi.org/10.1021/acs.cgd.8b00263.(c) Peña I, Sanz ME, Alonso E, Elena R, Alonso JL. The multiple hydrogen-bonding networks of polyol ribitol. *Eur J Chem*. 2018;24:13408–13412. https://doi.org/10.1002/chem.201803493.(d) Bifulco G, Dambruoso P, Gomez-Paloma L, Riccio R. Determination of relative configuration in organic compounds by NMR spectroscopy and computational methods. *Chem Rev*. 2007;107:3744–3779. https://doi.org/10.1021/cr030733c.(e) Higashibayashi S, Czechtizky W, Kobayashi Y, Kishi Y. Universal NMR Databases for Contiguous Polyols. *J Am Chem Soc*. 2003;125:14379–14393. https://doi.org/10.1021/ja0375481.(f) Hawkes GE, Lewis D. 1H nuclear magnetic resonance spectra and conformations of alditols in deuterium oxide. *J Chem Soc Perkin Trans*. 1984;2:2073–2078. https://doi.org/10.1039/P29840002073.(g) Angyal SJ, Le Fur R. The 13C-N.M.R. spectra of alditols. *Carbohydr Res*. 1980;84:201–209. https://doi.org/10.1016/S0008-6215(00)85551-2.
31. (a) Jenkinson SF, Booth KV, Gullapalli P, et al. 1-Deoxy-L-mannitol (6-deoxy-L-mannitol or L-rhamnitol). *Acta Cryst*. 2008;E64:o1705–o1706. https://doi.org/10.1107/S1600536808024586.(b) Jeffrey GA, Kim HS. Conformations of the alditols. *Carbohydr Res*. 1970;14:207–216. https://doi.org/10.1016/S0008-6215(00)80488-7.
32. Chaudhuri R, Prasanth T, Dash J. Expanding the toolbox of target directed bio-orthogonal synthesis. In situ direct macrocyclization by DNA templates. *Angew Chem Int Ed*. 2023;62, e202215245. https://doi.org/10.1002/anie.202215245.
33. (a) De Cian A, Guittat L, Kaiser M, et al. Fluorescence-based melting assays for studying quadruplex ligands. *Methods*. 2007;42:183–195.(b) Renciuk D, Zhou J, Beaurepaire L, Guédin A, Bourdoncle A, Mergny JL. A FRET-based screening assay for nucleic acid ligands. *Methods*. 2012;57:122–128. https://doi.org/10.1016/j.ymeth.2012.03.020.(c) Kieltyka R, Englebienne P, Fakhoury J, Autexier C, Moitessier N, Sleiman HF. A platinum supramolecular square as an effective G-

quadruplex binder and telomerase inhibitor. *J Am Chem Soc*. 2008;130: 10040–10041. https://doi.org/10.1021/ja8014023.
34. Suh D, Chaires JB. Criteria for the mode of binding of DNA binding agents. *Bioorg Med Chem*. 1995;3:723–728. https://doi.org/10.1016/0968-0896(95)00053-J.
35. Cohen G, Eisenberg H. Viscosity and sedimentation study of sonicated DNA–proflavine complexes. *Biopolymers*. 1969;8:45–55. https://doi.org/10.1002/bip.1969.360080105.
36. Fairley TA, Tidwell RR, Donkor I, et al. Structure, DNA minor groove binding, and base pair specificity of alkyl- and aryl-linked bis(amidinobenzimidazoles) and bis (amidinoindoles). *J Med Chem*. 1993;36:1746–1753. https://doi.org/10.1021/jm00064a008.
37. (a) Ren J, Chaires JB. Rapid screening of structurally selective ligand binding to nucleic acids. *Methods Enzymol.* 2001;340:99–108. https://doi.org/10.1016/S0076-6879(01)40419-8.(b) Chaires JB. Nucleic acid binding molecules: a competition dialysis assay for the study of structure-selective ligand binding to nucleic acids. In: Beaucage SL, Bergstrom DE, Glick GD, Jones RA, eds. *Current protocols in nucleic acid chemistry*. New York: John Wiley & Sons; 2002:831–838. https://doi.org/10.1002/0471142700.nc0803s11.(c) Chaires JB. Structural selectivity of drug-nucleic acid interactions probed by competition dialysis. In: Waring MJ, Chaires JB, eds. *DNA binders and related subjects. Topics in current chemistry 253*. Berlin, Heidelberg: Springer; 2005:33–53.
38. van Holde KE, Johnson WC, Ho PS. *Principles of physical biochemistry*. New Jersey: Prentice Hall; 1998.
39. Muller W, Crothers DM. Interactions of heteroaromatic compounds with nucleic acids. *Eur J Biochem*. 1975;54:267–277. https://doi.org/10.1111/j.1432-1033.1975.tb04138.x.
40. (a) Kaur G, Dwivedi Y, Rai SB. Synthesis, structural, thermal and optical studies of rare earth coordinated complex: $Tb(Sal)_3Phen$. *Mater Chem Phys*. 2011;130: 1351–1356. https://doi.org/10.1016/j.matchemphys.2011.09.028.(b) Paw W, Eisenberg R. Synthesis, characterization, and spectroscopy of dipyridocatecholate complexes of platinum. *Inorg Chem*. 1997;36:2287–2293. https://doi.org/10.1021/ic9610851.
41. (a) Jothi I, Alexander V. Organic NLO material with H-bonded 1D helical self-assembly: synthesis, X-ray crystal structure, DFT calculations, SHG measurements and thermal studies of (5Z,6E)-1,10-phenanthroline-5,6-dione dioxime. *CrstEngComm*. 2017;19:5251–5258. https://doi.org/10.1039/C7CE00743D.(b) Gebreyohannes BG, Chebude Y, Raju VJT. Synthesis and Characterization of Metal Complexes of Derivative of 1,10-phenanthroline. *Int Res J Pure Appl Chem*. 2016;12: 18137. https://doi.org/10.9734/IRJPAC/2016/18137.(c) Das O, Paria S, Zangrando E, Paine TK. Copper(II)-mediated oxidative transformation of vic-dioxime to furoxan: evidence for a copper(II)-dinitrosoalkene intermediate. *Inorg Chem*. 2011;50:11375–11383. https://doi.org/10.1021/ic200979q.(d) Kleineweischede A, Mattay J. Synthesis of amino- and bis(bromomethyl)-substituted bi- and tetradentate N-heteroaromatic ligands: building blocks for pyrazino-functionalized fullerene dyads. *Eur J Org Chem*. 2006:947–957. https://doi.org/10.1002/ejoc.200500548.(e) Bodige S, MacDonnell FM. Synthesis of free and ruthenium coordinated 5,6-diamino-1,10-phenanthroline. *Tetrahedron Lett*. 1997;38: 8159–8160. https://doi.org/10.1016/S0040-4039(97)10223-4.
42. Chou SP, Juan J, Tsay S, Huang KP, Hwu JR. Oxime esters of 2,6-diazaanthracene-9,10-dione and 4,5-diazafluoren-9-one as photo-induced DNA-cleaving agents. *Molecules*. 2012;17:3370–3382. https://doi.org/10.3390/molecules17033370.
43. Pennarun G, Granotier C, Gauthier LR, et al. Apoptosis related to telomere instability and cell cycle alterations in human glioma cells treated by new highly selective G-quadruplex ligands. *Oncogene*. 2005;24:2917–2928. https://doi.org/10.1038/sj.onc.1208468.